Final Project report

Understanding the distribution of lithologies in Zechstein salt diapirs and their impact on quantifying subrosion in the Netherlands for the safety of nuclear waste disposal repositories

Authors:

A. Auzemery[1],

L. Matenco[1],

Marie-Christine Cacas[2],

F. H. Nader[1,2],

J. Bartol[3],

F. Beekman[1]

Consortium: Utrecht University and IFP Energies Nouvelles Beneficiary:

Ministry of Infrastructure and Water Management

November 2025

Corresponding author: Antoine Auzemery (a.auzemery@uu.nl)

[1] Utrecht University, Faculty of Geosciences, Department of Earth Sciences.

[2] IFP Energy Nouvelles, France

[3] Centrale Organisatie Voor Radioactief Afval (COVRA), the Netherlands

Executive Summary

This report presents the results of a 6-month extension of the 2024 joint UU–IFPEN–COVRA project (Li et al., 2024), which developed the first generation of quantitative models of the long-term geological and hydrological evolution of Zechstein salt diapirs in the Netherlands. In the previous phase, geological, well and seismic data were compiled into 3D structural models using TemisFlow™ software and long-term salt movement was simulated. In these models, the Zechstein was represented as a single lithology composed entirely of salt, with no distinction between intra-salt layers, and hydrodynamic parameters were not constrained by measured data. The current follow-up project focused on better constraining the lithological variability within Zechstein salt diapirs and increasing the resolution of the previous model by integrating geological, hydrodynamic and salinity data. The project comprised two work packages: (1) detailed characterisation of the intra-Zechstein litho-stratigraphy across the Netherlands and (2) hydro-chemical modelling of diapir subrosion.

In the first work package, relevant Zechstein data from available reports, borehole logs and seismic data at 92 boreholes that penetrated the Zechstein at depth beneath 1000 metres were retrieved, quality-checked and integrated. At each location, the Zechstein interval was divided into subunits, employing a newly developed lithology-based classification scheme. The descriptions of the type and thickness of each Zechstein subunit are made available in a structured database and metadata catalogue in Excel format. The new Zechstein data are presented on regional maps as local lithological thickness columns. Furthermore, we have used the entire Netherlands public database to create two new maps based on 1994 corrected wells showing the total salt thickness and total non-salt thickness within the Zechstein interval. These maps show large variations in thicknesses with the regional trends in salt thickness being markedly different when compared with previous total Zechstein thickness models. A large number of salt diapirs were found to be capped by non-salt layers forming a distinct caprock unit at the top of the structure. Comparing the burial depth and caprock thickness of many diapirs suggests that caprock thickness decreases with increasing depth.

In the second work package, the TemisFlow™ hydro-geochemical modelling software was used to study subrosion of Zechstein salt diapirs. The updated geological model was combined with revised lithologies, hydrodynamic boundary conditions from the national REGIS II groundwater model and salinity distributions from the NHI framework. Focus was given to the implementation of caprock lithologies, allowing the model to account for their influence on dissolution processes and fluid transport. Conceptual models were first developed to evaluate the sensitivity of subrosion to individual parameters such as caprock thickness, porosity, aquifer salinity and groundwater flow. These simulations provided estimates of subrosion rates of different orders of magnitudes and helped isolate the main controlling factors. Based on the conceptual results, a real-case scenario model was developed for the northern Netherlands, incorporating the detailed lithological data from the first work package and implementing caprocks for the major diapirs. The model produced 3D estimates of past subrosion over the last million years, as well as potential future dissolution over the next million years. Results show that previous models without caprock implementation substantially overestimated

subrosion, predicting rates up to ~150 metres per million years (m /Myr), whereas the inclusion of realistic caprock properties reduces significantly the subrosion to possibly only a few meters per million years in the conditions of our modelling. However, the error bars of our estimates are still in the order of at least one orders of magnitude due to the generic implementation of hydrodynamic conditions, diapir geometry and caprock composition at the entire large scale of the northern Netherlands. Positively, the modelling demonstrates that when local conditions of each diapir are accounted in specific modelling, then the errors bars are significantly reduced to metres per million years, which is a resolution needed to analyse the safety of nuclear waste disposal repositories. This specific local modelling for all sites is recommended as the next step in a future project. The outputs of this work package include a 3D model in TemisFlow™, and maps of subrosion rates, delivered in xyz grid format.

Introduction to subrosion processes in Zechstein salt diapirs

Rock salt offers a combination of impermeability, ductile deformation and self-sealing capacity, making it a potentially suitable host rock for the geological disposal of nuclear waste (Bartol & Vuorio, 2025; Gerard & Wildenborg, 1999; Kothe et al., 2007). In the Netherlands, potential disposal sites are associated with the Zechstein salt formations, which comprise thick, laterally extensive layers and diapiric structures distributed across the northern and eastern onshore regions and the adjacent offshore domain (Geluk et al., 2007; Lang et al., 2014; Li et al., 2024).

Over geological time, the Zechstein salt has undergone diapiric uplift and formed pillows and domes that pierce through the overlying Mesozoic and Cenozoic sediments. This upward movement is driven by the low density and viscous rheology of salt under differential loading and tectonic stress (Daudré & Cloetingh, 1994; Jackson & Hudec, 2017). Estimated long-term diapiric rise rates in the Netherlands range from 0.001 to 0.1 mm/yr (Lauwerier, 2022; Almalki, 2023), with episodic accelerations during the Late Cretaceous (Remmelts et al., 1993; Li et al., 2024). These processes have created thick accumulations of salt, that are potentially suitable for the disposal of radioactive waste.

However, the integrity of these salt formations may be affected by subrosion. Subrosion is the dissolution of salt by groundwater circulation near the top or flanks of diapirs. Subrosion progressively removes halite K-salt and soluble elements, and may lead to collapse, fracturing, or enhanced permeability in the diapir or the overlying sediments (Prij et al., 1993; Al-Halbouni et al., 2017). Although many shallow diapirs present adequate volumes and accessibility for a repository design, they are also more exposed to groundwater flow and thus more susceptible to subrosion, especially in areas influenced by meteoric recharge and freshwater aquifers (Kothe et al., 2007). Understanding the extent and rate of subrosion is therefore essential for evaluating the long-term safety of nuclear waste disposal in a salt dome.

Modelling results from the previous UU–IFPEN–COVRA collaboration (Li et al., 2024) demonstrated that, for relatively pure halite systems, subrosion is primarily localized at the diapir crests, where fluid flow and hydraulic gradients have the highest values. The simulations also indicated that the salinity of circulating fluids significantly influences dissolution intensity—higher salinity reduces dissolution potential—while at greater depths, the limited hydraulic connectivity results in negligible subrosion. These findings highlight the importance of constraining hydrodynamic and geochemical conditions when evaluating the long-term evolution of salt diapirs.

At the interface between the dissolving salt and the overlying sediments, the insoluble residues left behind by subrosion commonly accumulate to form a caprock. This material typically consists of primary anhydrite and gypsum, but also, dolomite, and variable amounts of clay or marl, representing the non-soluble components of the original evaporitic sequence (Geluk et al., 1993; Lang et al., 2014). Caprocks can act as secondary barriers to fluid flow, but their heterogeneity and variable thickness—ranging from a few metres to several tens of metres—reflect the intensity and duration of dissolution processes. Their composition and structure provide valuable indicators of past subrosion activity and are critical for assessing the current stability of the diapir system.

In addition to caprocks, the internal composition of Zechstein salt is another key factor influencing the mechanical and geochemical behaviour of diapirs. The Zechstein is not made up entirely of pure halite, but contains other types of salt and numerous non-salt intercalations, such as anhydrite, carbonates and clay-rich layers, inherited from the original evaporitic stratigraphy (Hunfeld et al., 2023). These layers introduce heterogeneity in mechanical strength, permeability and dissolution potential, which can influence both diapiric evolution and subrosion patterns.

Therefore, a detailed understanding and mapping of intra-Zechstein lithologies are crucial to reduce uncertainties in geological and numerical models of salt diapirs. Variability in caprock and non-salt intercalations directly influences subrosion processes, creating feedback mechanisms that affect diapir stability and fluid flow. Key questions include how these lithologies vary both laterally and with depth, and how they influence susceptibility to subrosion. It is also essential to identify where shallow, high-purity salt is present. By integrating well, seismic and petrophysical data, the variability in non-salt intercalations and caprock lithologies can be better constrained, providing the foundation for refined numerical simulations of diapir stability, subrosion and hydrodynamic evolution—key components in assessing the suitability and long-term safety of Zechstein salt structures for nuclear waste disposal in the Netherlands.

This report is structured in two main parts. Part I (WP1) presents the lithological characterization of the Zechstein diapirs in the Netherlands, focusing on the identification and spatial distribution of salt and non-salt lithologies and the development of updated thickness maps. Part II (WP2) builds on this geological foundation, addressing the hydrodynamic parametrization and modelling of subrosion processes in the northern Netherlands, where the influence of caprock properties, aquifer salinity and fluid dynamics on salt dissolution and stability is quantitatively assessed. Together, these two parts provide a comprehensive understanding of the geological and hydrodynamic controls governing subrosion and the long-term integrity of Zechstein salt structures.

WP1 – Lithological Characterization of the Zechstein Diapirs in the Netherlands

1. Inventory of Zechstein intra-salt lithologies based on Well Data

1.1 Objectives

The inventory aims to compile, evaluate and harmonize all available geological, geophysical and other datasets relevant to the characterization of lithological heterogeneity within Zechstein salt structures in the Netherlands. The work focuses on improving the consistency and completeness of lithological, stratigraphical and petrophysical data used for subsequent structural and numerical modelling. The boundary conditions for the project were defined by COVRA, with a focus on salt located above 1000 m depth below sea level and Zechstein layers with a thickness greater than 100 m.

1.2 Methodology

The initial stratigraphic and lithological data were obtained from the TNO DGMv5 model. To improve and refine this dataset, additional information was collected through detailed analysis of well reports (via NLOG and DINOloket), well logs (gamma-ray, density and sonic) and seismic data. A total of 92 wells meeting the boundary conditions were analysed, including 75 onshore wells and 17 offshore wells (North Sea) (Fig. 1). The onshore wells with Zechstein shallower than 1000 m are mainly located in the northern and eastern parts of the Netherlands, whereas the offshore wells are concentrated in the northern offshore domain (Fig. 1). All datasets were then integrated, updated and corrected as necessary, ensuring consistency in depth references, coordinate systems and lithological classifications. The updated information was further integrated into the broader geological framework, linking well data, intra-salt layers and regional stratigraphy.

To standardize the interpretation of lithological intervals, the stratigraphic codes provided by NLOG were reclassified into simplified lithological categories. The classification followed a rule-based scheme in which each interval's lithostratigraphic code was mapped to a representative lithology. Intervals labelled as faults were identified first and excluded from lithological analysis. Zechstein units (codes beginning with "ZE") were then grouped according to their dominant mineralogy and depositional characteristics, while all other intervals were classified as non-Zechstein (grey lithologies in the well-log data). The Zechstein codes were assigned to lithological classes (Table 1). The resulting database provides standardized lithological profiles and an inventory of intercalations by rock type and thickness.

In this study, the Zechstein sequence and associated formations are further classified into three main categories to distinguish salt and caprock from other lithologies (Table 2).

Code prefix or identifier	Lithological class	Description	Representative color (used in figures)
ZEUC, ZECP	Caprock / Upper clay	Clay-rich to gypsiferous caprock units	Brown
ZESA, ZESAU, ZESAL, or codes ending in H	Salt (Halite)	Halite-dominated layers (>90% halite)	Magenta
ZEZ1A, ZEZ1W, ZEZ1T, ZEZ2A, ZEZ3A, ZEZ4A, ZEZ2T	Anhydrite	Massive anhydrite or mixed anhydrite–halite facies	Purple
ZEZ1C, ZEZ1F, ZEZ2C, ZEZ3C	Carbonate	Dolomitic and calcareous layers	Turquoise
ZEZ1G, ZEZ1M, ZEZ2M, ZEZ1K, ZEZ3U	Claystone	Clay- and marl-rich units	Dark green
ZEZ3G	Grey salt clay	Halitic–argillaceous facies	Grey-green
ZEZ4R	Red salt clay	Halitic facies rich in red clays or iron oxides	Dark red
Other Zechstein codes	Other Zechstein	Undifferentiated or mixed lithologies	Dark blue
Non–Zechstein codes	Non-Zechstein	Overburden or pre-Zechstein strata	Grey
Fault	Fault zone	Structural discontinuities	Black

Table 1. *Simplified lithological classification of Zechstein and non-Zechstein units based on NLOG stratigraphic codes, with corresponding color scheme used in log profiles. This color-coded classification captures the main lithological contrasts within the Zechstein Group—halite, anhydrite, carbonate, clay-rich and caprock facies—allowing direct visual comparison between wells in subsequent plots.*

Category	Description	Typical Codes	Color in Figures
Salt	Halite-dominated layers (>90% halite or K-salt)	ZESA, ZESAU, ZESAL, or codes ending in H	Magenta
Caprock / Upper clay	Clay-rich to gypsiferous layers overlying salt	ZEUC, ZECP	Brown
Non-Salt	Carbonate, clay, sandstone, marls.	All other lithologies	Dark Blue

Table 2. *Summary of Salt Non-Salt and Caprock lithological categories used in this study, including their definitions, coding conventions, and color representation in histograms.*

1.3 Output

A structured database and metadata catalogue, delivered in XLS (tabular), suitable for direct integration into Petrel™, TemisFlow™ models and GIS software. All tables are in a zip file, one for offshore wells and one for onshore wells, containing the image log in PNG and the stratigraphic and lithological information for each well (Appendix 1).

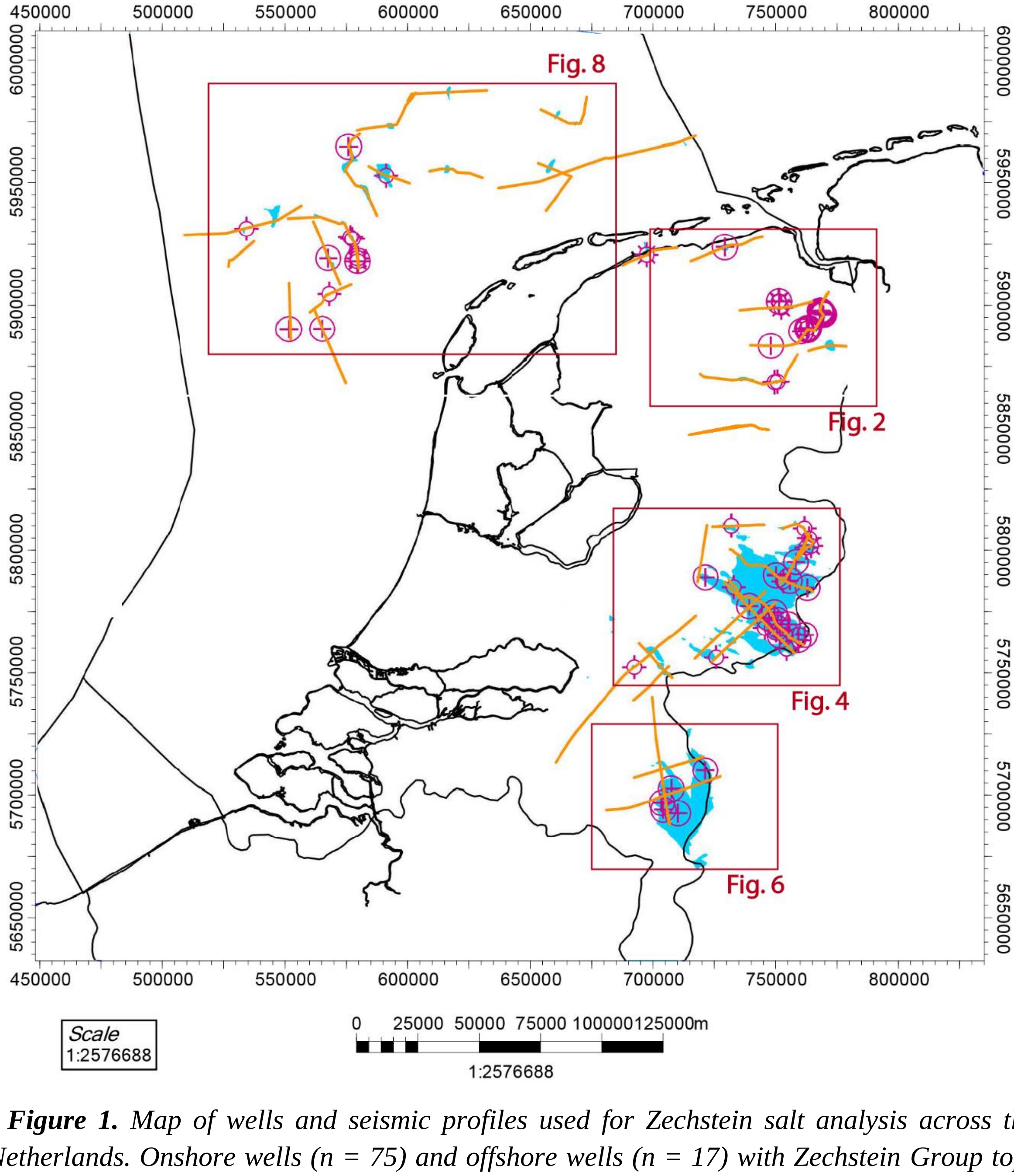

Figure 1. *Map of wells and seismic profiles used for Zechstein salt analysis across the Netherlands. Onshore wells (n = 75) and offshore wells (n = 17) with Zechstein Group tops shallower than −1000 m are shown in magenta. The blue shading indicates regions where the Zechstein occurs shallower than −1000 m. Seismic lines used to guide the study are highlighted in orange. This dataset integrates TNO DGMv5 stratigraphy with additional well data from NLOG, DINOloket, and well logs (gamma-ray, density, sonic) to refine lithological interpretations. Red squares indicate the outline of the area shown in the figure presented in Section 1.*

1.4 Results

The results are presented by region across the Netherlands. For each region, an inventory of lithologies within Zechstein salt diapirs was compiled from available well data. Given the −1000 m project boundary, the analysis was extended to −1200 m to include a 200 m depth margin, allowing intervals just below the limit to be represented and ensuring complete coverage of Zechstein thicknesses near the boundary. For each region, the following are provided:

- A map showing the cumulative thickness of Salt, Non-Salt and Caprock lithologies at each well, displayed using histogram bars.
- Selected seismic profiles representative of the regional diapiric structures, correlated with well-based lithological interpretations.

1.4.1 Northern Onshore Netherlands (Groningen, Friesland, Drenthe)

The northern Netherlands hosts the thickest Zechstein sequences and the largest salt diapirs in the onshore domain, exceeding 2000 m in thickness and extending across the eastern part of the study area (Figs. 2–3). These diapirs are well developed, displaying tall and mature salt intrusions that penetrate Mesozoic and Cenozoic formations. They consist predominantly of massive halite, overlain by a caprock composed of non-soluble lithologies (anhydrite, carbonate, or claystone) with variable thicknesses ranging from 5 to 80 m. Non-salt intercalations within the salt are generally limited. Notable examples include the Pieterburen and Ternaard diapirs, with tops located at approximately -750 m and -250 m depth, respectively (Fig. 3a). Despite their close proximity, they differ markedly in caprock thickness — about 13 m for Ternaard and 90 m for Pieterburen (Figs. 2 and 3a) — illustrating strong lateral variability in caprock development even over short distances.

Further south, a series of massive diapirs: Anlo, Zuidwending, Winschoten, Onstwedde and Schoonloo (Fig. 2 and Fig. 3) display broadly similar characteristics. In these structures, caprock and non-salt lithologies are generally confined to the uppermost 50 m, underlain by thick, relatively homogeneous halite bodies with few anhydrite intercalations. Compositional logs indicate that the salt consists of 2–8% non-soluble elements, with the remaining fraction dominated by halite. However, the dense well coverage over the Zuidwending and Winschoten diapirs reveals significant variation in caprock thickness along strike, indicating that geological heterogeneity is high along the top of these diapirs (Fig. 2). These diapirs also exhibit the thickest caprocks observed in the dataset, ranging from 20 m to 80 m, suggesting spatially variable but locally enhanced subrosion within the region. It is also noteworthy that the caprock is significantly thicker at the crest of diapirs than along their flanks. For example, at the Schoonloo diapir (Fig. 3, profile b), well SOL-02, located on the diapir crest, contains a ~34 m-thick caprock, whereas well SOL-01, positioned on the flank, shows only ~4 m of caprock.

While the northern diapirs contain pure salt near the surface, the variability in caprock thickness at their crests suggests that subrosion processes may have been significant. Their relatively shallow depth and potential interaction with freshwater aquifers make them more susceptible to subrosion.

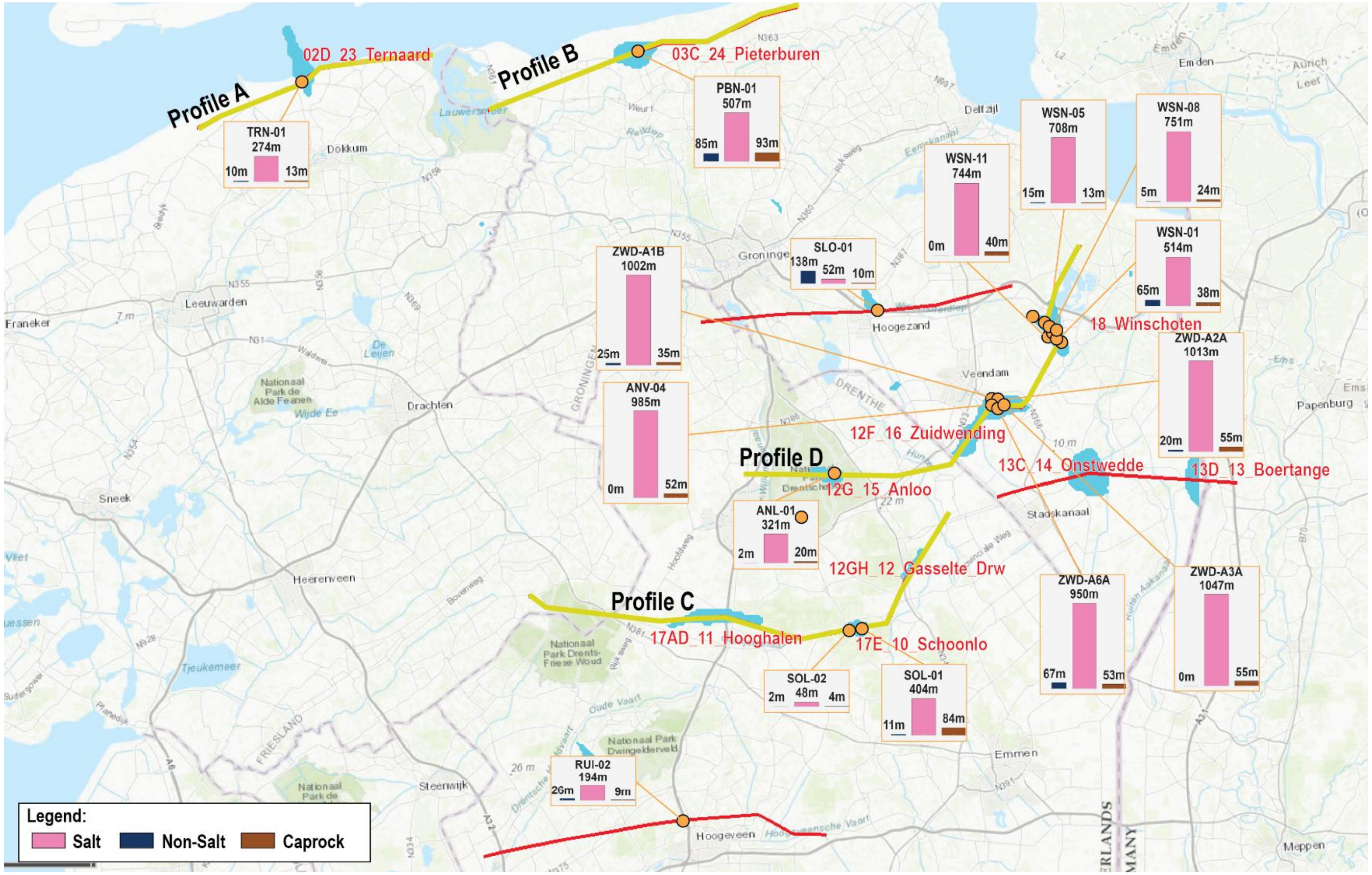

Figure 2. *Inventory of lithologies within Zechstein salt diapirs derived from well data in the Northern Netherlands (Groningen, Friesland, Drenthe). The map displays cumulative thicknesses of Salt, Non-Salt, and Caprock lithologies within the Zechstein interval above −1200 m depth, reflecting the depth threshold of 1000m + 200m margin currently applied, consistent with current discussions on deep geological disposal. The blue shading indicates regions where the Zechstein occurs shallower than −1200 m, red lines are locations of seismic profiles used to guide the study, and yellow lines mark the locations of seismic profiles shown in Figure 3.*

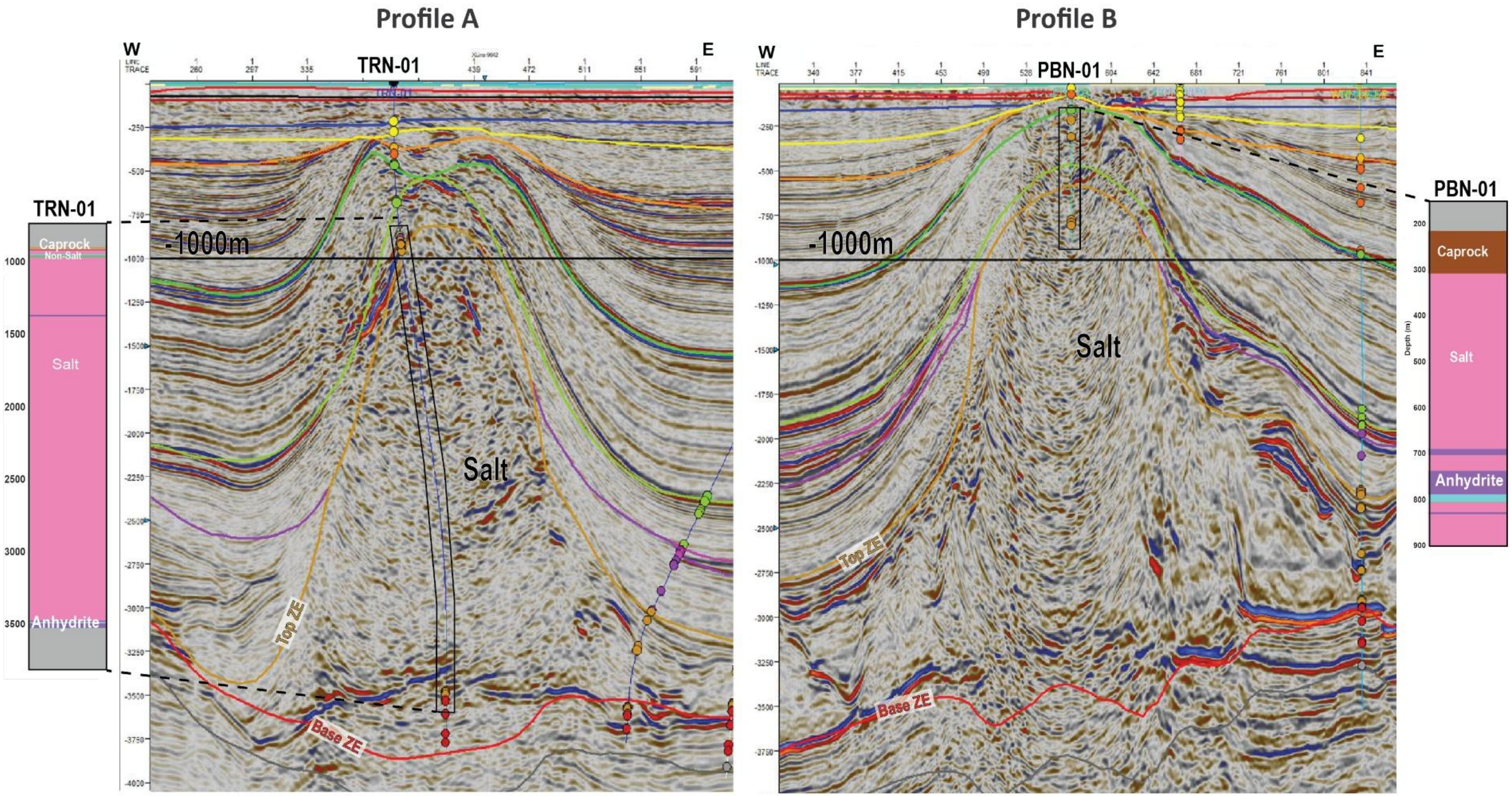

Profile A
Profile B
W
E
TRN-01
PBN-01
-1000m
Salt
Top ZE
Base ZE
Caprock
Non-Salt
Anhydrite

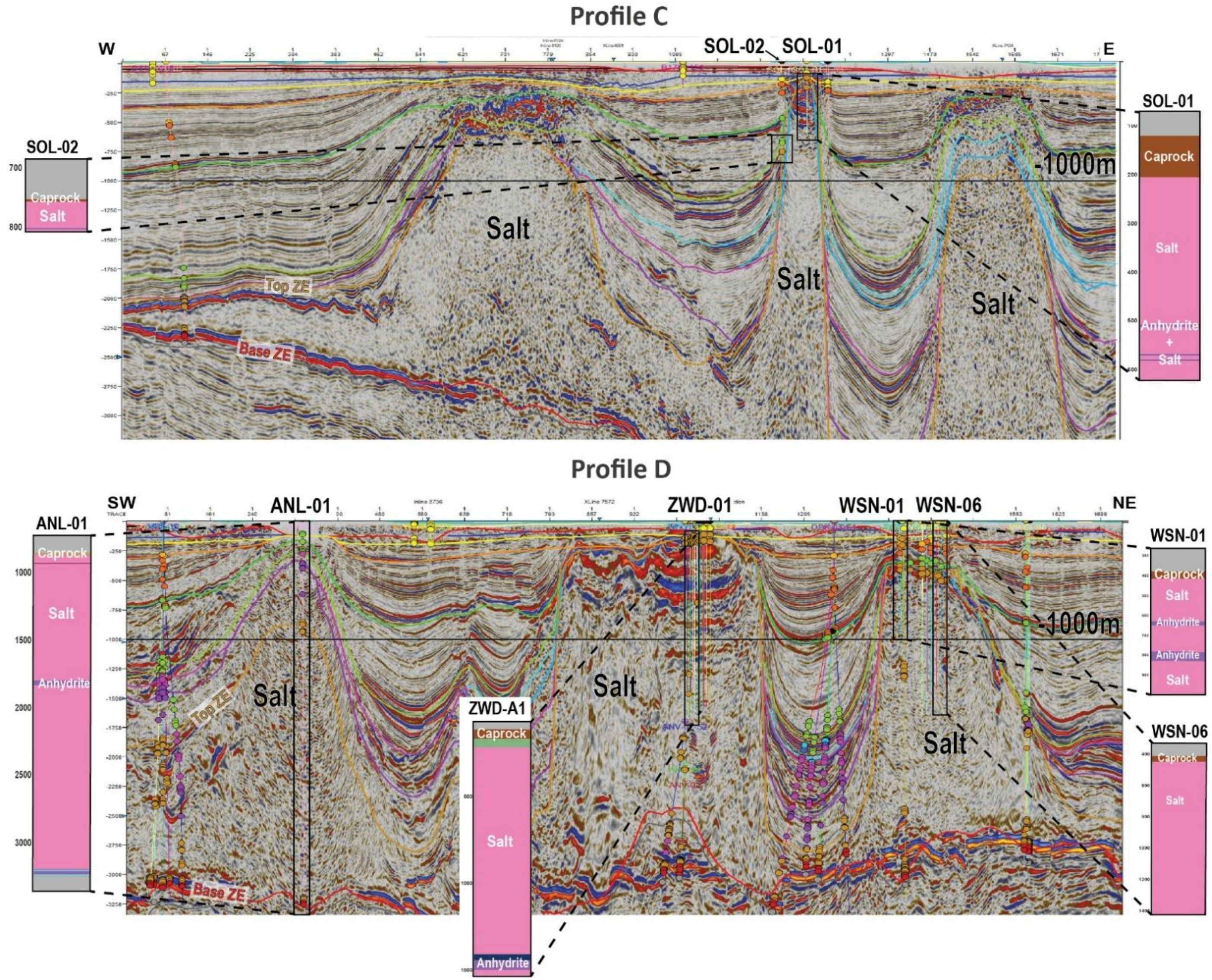

Profile C
W
E
SOL-02
SOL-01
Caprock
Salt
Anhydrite + Salt
-1000m
Top ZE
Base ZE
Profile D
SW
NE
ANL-01
ZWD-01
WSN-01
WSN-06
ZWD-A1
Anhydrite

Figure 3. *Interpretation of Zechstein lithologies based on well data along seismic profiles A–D (see location in Fig. 2). The northern Netherlands is characterized by numerous large diapirs exceeding 2000 m in thickness. These structures exhibit thick halite cores, overlain by caprocks of variable thickness (5–80 m), and only limited non-salt intercalations. The sections illustrate the strong lateral variability in caprock development, as seen between the Pieterburen and Ternaard diapirs, and highlight that mature diapirs such as Zuidwending and Winschoten are dominated by thick, uninterrupted halite sequences.*

1.4.2 Eastern Onshore Netherlands (Overijssel and Gelderland)

In the eastern Netherlands, the Zechstein salt occurs as a series of relatively small salt pillows, typically less than 400 m thick and situated at depths of approximately 400–1200 m (Figs. 4–5). These structures are less well developed and smaller in scale compared to the large northern diapirs. They are characterized by numerous non-salt intercalations, particularly near the top and frequent anhydrite bands, resulting in a more heterogeneous lithological composition within the salt bodies (Fig. 5).

Despite their limited vertical thickness, several salt structures contain substantial accumulations of pure salt, with layers locally exceeding 200–300 m. Salt is often interlayered with anhydrite, carbonate and minor claystone intercalations. Caprock thickness above these structures is generally thinner than in the northern Netherlands, averaging 10–30 m. High-quality seismic data to the north of the area indicate that the HEN-01 well intersects a small salt pillow containing a 220 m thick salt layer. Seismic profiles E and F, correlated with well data (Fig. 5), show that the internal architecture of these small pillows is highly variable. Wells HGL-01 and ISH-01, located on the flanks of the same salt pillow as HEN-01, intersect significantly more non-salt lithologies and considerably less salt. This suggests that salt is concentrated toward the center of the dome, while the composition of the flanks is more heterogeneous, highlighting the lateral variability within these small salt structures. Several other salt structures are present in this region but are only partially or not fully cored (e.g., BUS-01, DEW-03). Further south, the quality of seismic data decreases and interpretation of salt geometry becomes more unreliable; WSK-01 shows the thickest salt layer (320 m) in the south at 870 m depth.

The region is also characterized by numerous major faults, with wells frequently intersecting fault zones (e.g., GEL-01, PLG-01, WLO-01), which could affect the disposal potential of the salt.

Overall, the eastern salt structures represent smaller but important structures, containing high-purity salt at shallow depths. However, as demonstrated by the newly acquired reprocessing of SCAN lines, the presently mapped geometries of the Zechstein are highly unreliable. Advancing the understanding of the many small Zechstein salt accumulations requires targeted acquisition of new 3D seismic data.

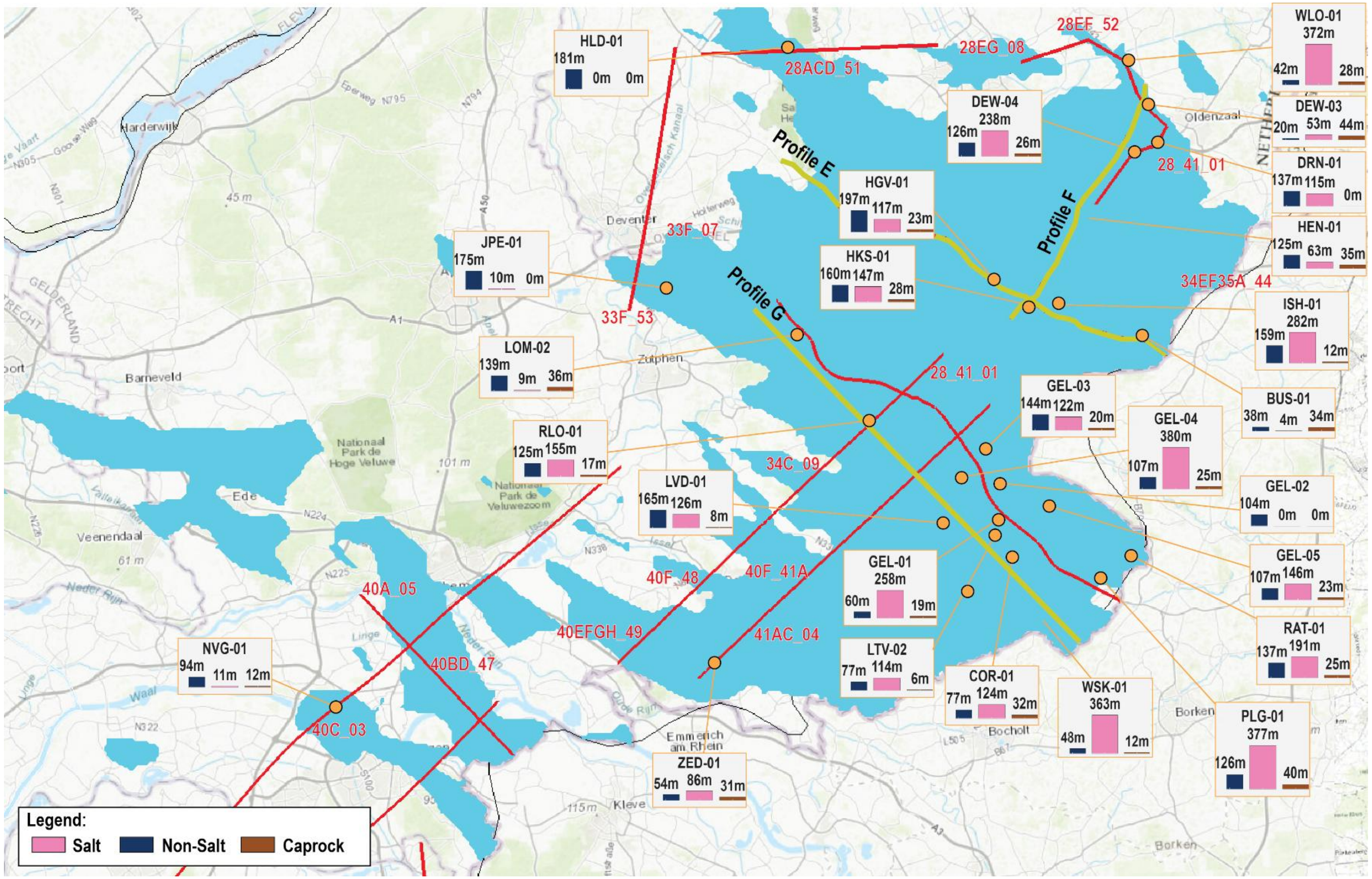

Figure 4. *Map of Zechstein salt structures in the Eastern Netherlands (Overijssel and Gelderland), showing the cumulative thickness of Salt, Non-Salt, and Caprock lithologies from well data above −1200 m depth. The map highlights numerous smaller diapiric structures (<400 m thick). Red lines are locations of seismic profiles used to guide the study, and yellow lines indicate the location of seismic profiles in Figure 5.*

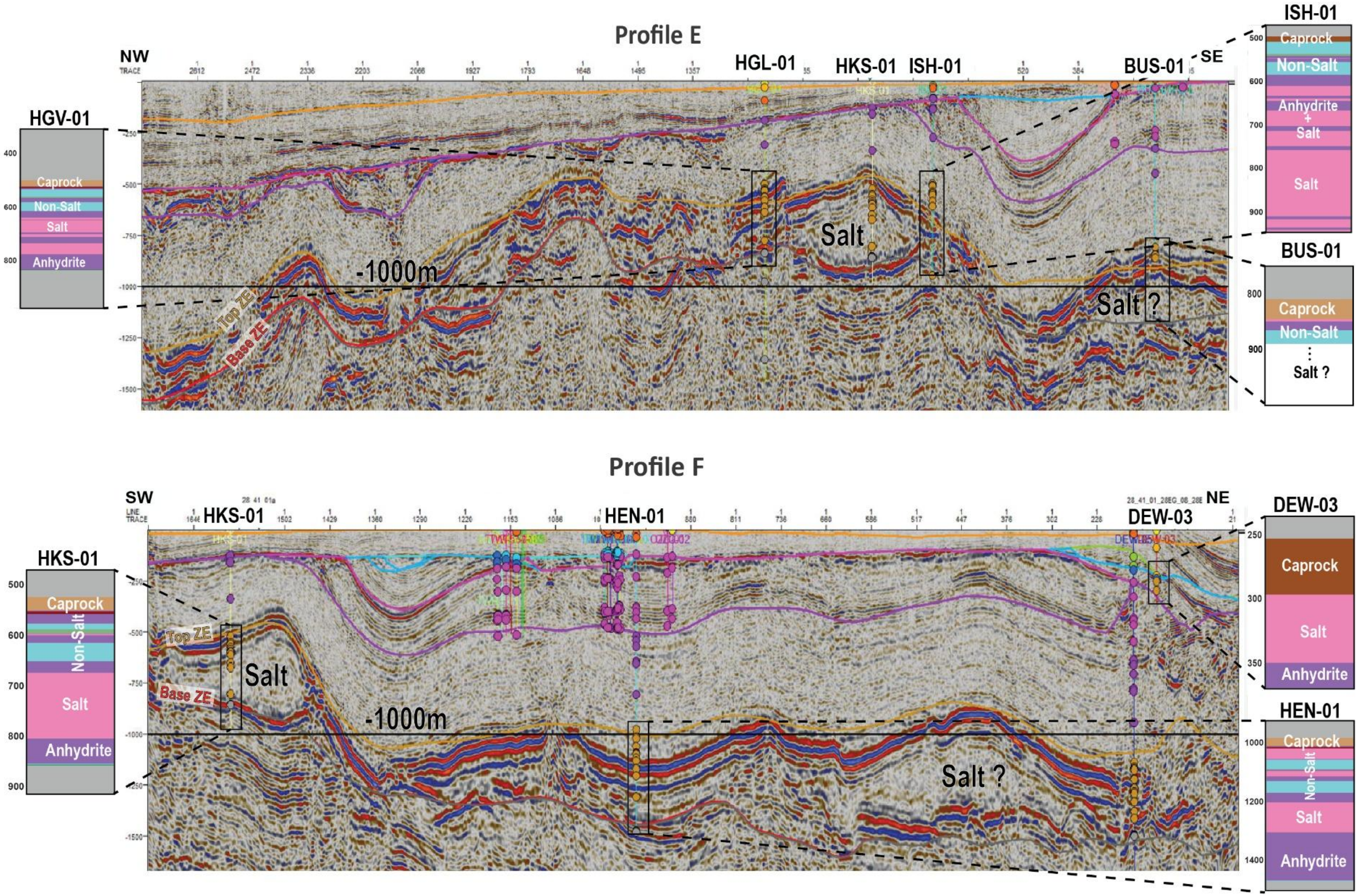
Profile E
NW
SE
HGL-01
HKS-01
ISH-01
BUS-01
HGV-01
Caprock
Non-Salt
Salt
Anhydrite
Anhydrite + Salt
Salt ?
-1000m
Top ZE
Base ZE
Profile F
SW
NE
HKS-01
HEN-01
DEW-03
Caprock
Non-Salt
Salt
Anhydrite
Salt ?
-1000m
Top ZE
Base ZE

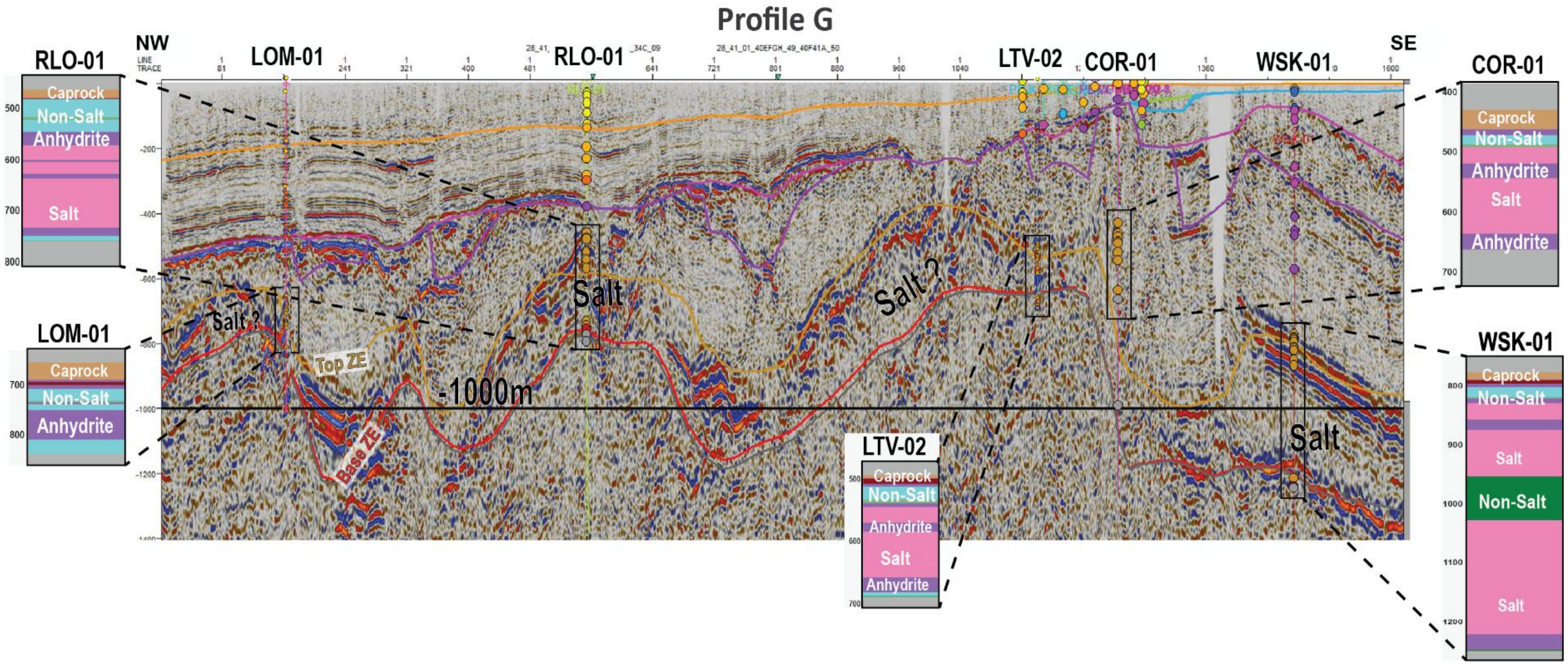

Figure 5. *Seismic profiles E, F and G, correlated with lithological logs from wells in the eastern Netherlands (see location in Fig. 4). The sections reveal small, heterogeneous salt structures composed of alternating salt and non-salt layers, including anhydrite and carbonate intercalations. Variability in internal architecture is evident between central and flank positions of diapirs (e.g., HEN-01 vs. ISH-01), emphasizing strong lateral lithological contrasts.*

1.4.3 South-Eastern Onshore Netherland (Brabant – Limburg)

In the south-eastern Netherlands, the Zechstein sequence is generally thin, undeformed and concordant, showing little evidence of salt tectonic activity. Salt mapping using seismics is highly unreliable with the present dataset. The succession is relatively flat-lying and conformably layered with the overlying formations. At depths of approximately 700–1200 m, the Zechstein interval is very thin—typically less than 80 m. Well data (ARC-01, ACA-11, HEL-05, CAL-GT-04, MRS-18) shows that the Zechstein layer is dominated by non-salt lithologies, primarily carbonates with minor clay intercalations (Fig. 6).

The Zechstein sequence thins toward the south, reflecting its position increasingly further from the Southern Permian Basin and closer to the Variscan orogen (e.g., Southern Permian Basin Atlas (2010)). Seismic data reveal very few indications of salt mobilization; however, a small structure near well CAL-GT-04, around seismic point 15199, may represent a remnant diapiric feature (Fig. 7).

Overall, the south-eastern Zechstein displays minimal potential for salt-based disposal, as the sequence is thin, largely non-evaporitic. Nevertheless, its well-preserved and conformable stratigraphy provides insight into the southern facies transition of the Zechstein Basin—likely situated near the Nijmegen area—where salt-dominated units give way to carbonate-dominated intervals.

1.4.4 Off-shore Netherlands

In the offshore Netherlands, the Zechstein salt diapirs exhibit characteristics broadly similar to those of the northern onshore region, with numerous large diapiric structures occurring at relatively shallow depths (300–1200 m). These offshore diapirs contain very thick sequences of nearly pure salt, with non-salt lithologies largely concentrated at the tops of the structures. The caprock in this domain is generally thinner than in the northern onshore diapirs, ranging from 10–20 m (Fig. 8), possibly reflecting the deeper position of the diapir tops or the reduced hydrodynamic activity in the offshore environment. However, many of the diapirs are not drilled, and interpreting the distribution between salt and caprock based solely on seismic data remains highly uncertain given the existing data.

Despite their favorable lithological characteristics, these diapirs are located relatively far offshore, with the first wells situated approximately 50 km from the coast. This distance introduces technical challenges for potential exploration or monitoring, though the geometries and internal compositions of the diapirs remain of interest. For example, the K18-09 and L13-03 wells intersect two diapirs with tops at ~700 m depth and thin caprocks (~5 m). K18-09 displays minimal non-salt intercalations, whereas L13-03 is more heterogeneous, with numerous anhydrite bands within the salt layer (Fig. 9).

Further north, a succession of diapirs (wells L10-C, L10-12, L10-16) top at 500–550 m and shows very high thicknesses of pure salt, with caprocks ranging from 5–25 m and only minor non-salt intercalations. Notably, although L10-12 and L10-16 are located on the same diapir, L10-16 contains significantly more limestone intercalations, illustrating the high lateral variability within individual diapirs.

Overall, the offshore diapirs are characterised by a high-purity salt content, relatively shallow depths and limited non-salt intercalations. The thinner caprocks suggest reduced hydrodynamic activity and potentially lower subrosion rates compared to onshore diapirs. However, the offshore environment involves specific practical challenges.

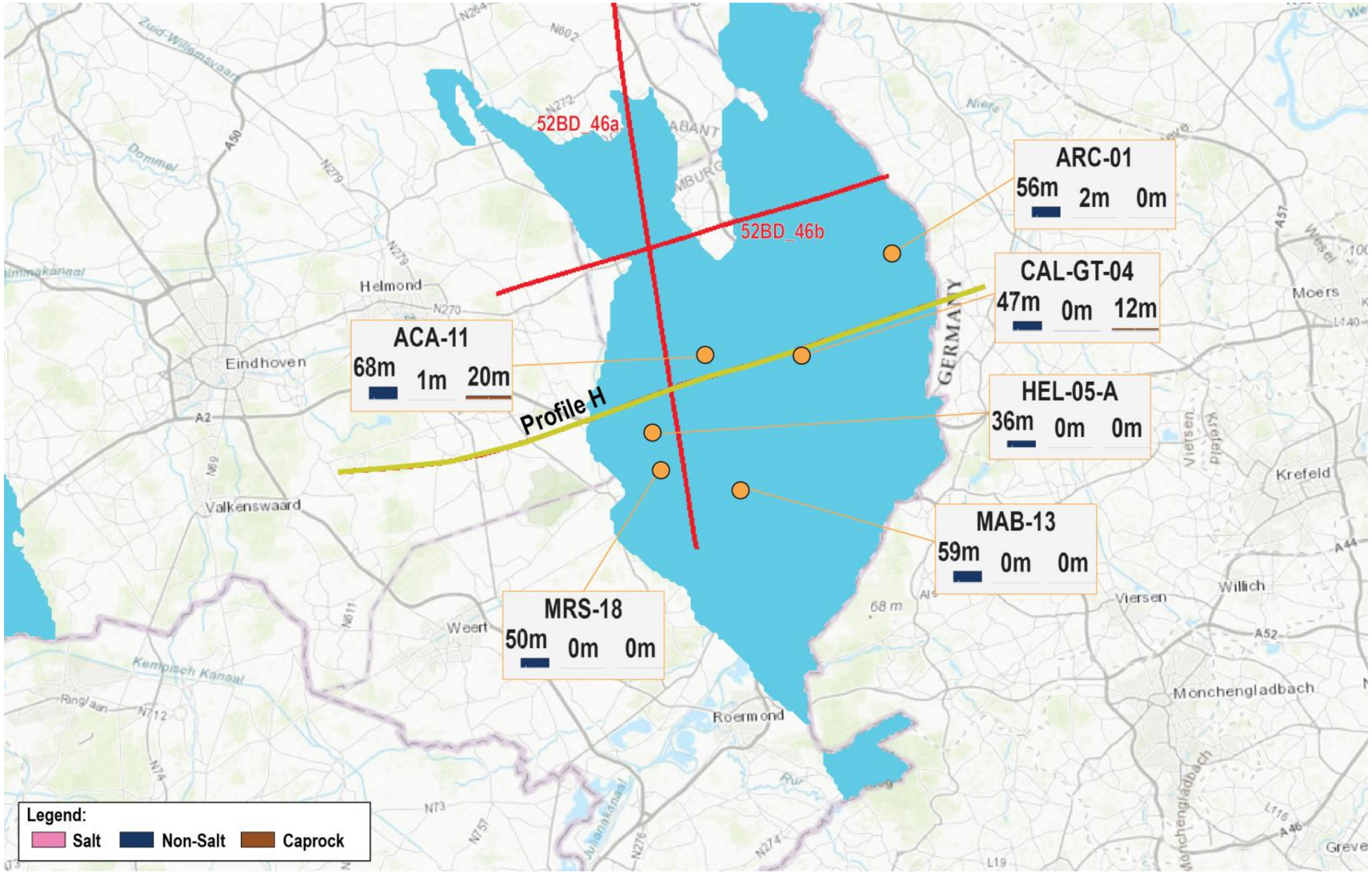

Figure 6. *Distribution of Zechstein lithologies in the South-eastern Netherlands (Limburg region). The map shows the thin, largely undeformed Zechstein interval (<80 m) between 700–1200 m depth, dominated by carbonate and minor claystone lithologies. The absence of significant salt accumulations indicates a transition from evaporitic to non-evaporitic facies toward the southern basin margin. Red lines are locations of seismic profiles used to guide the study and yellow lines indicate the locations of seismic profile H shown in Figure 7.*

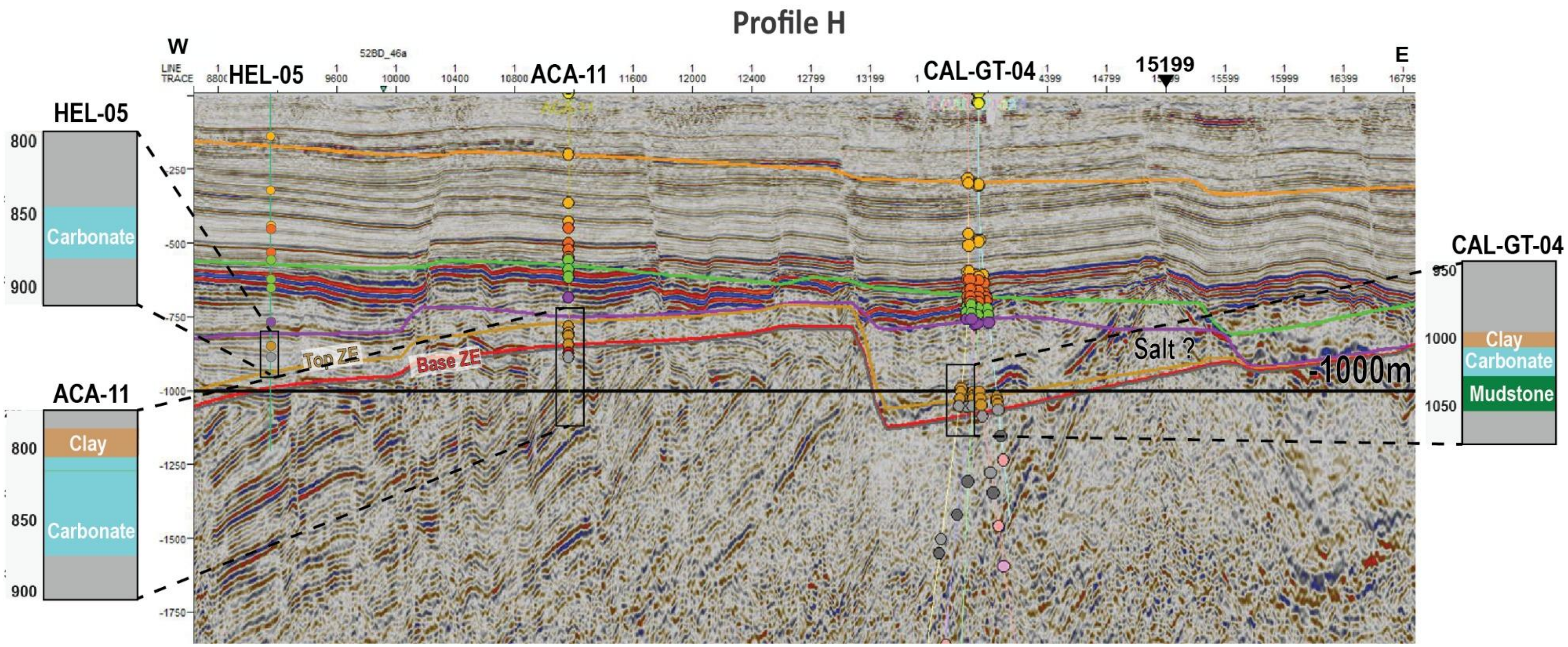

Figure 7. Seismic profile H, intersecting well CAL-GT-04 in the south-eastern Netherlands (see location in Fig. 6). The section reveals a sub horizontal, undeformed Zechstein sequence with limited evidence of salt mobilization. A small structure near seismic point 15199 is interpreted as a remnant diapiric feature, marking the southernmost occurrence of Zechstein deformation in the onshore domain.

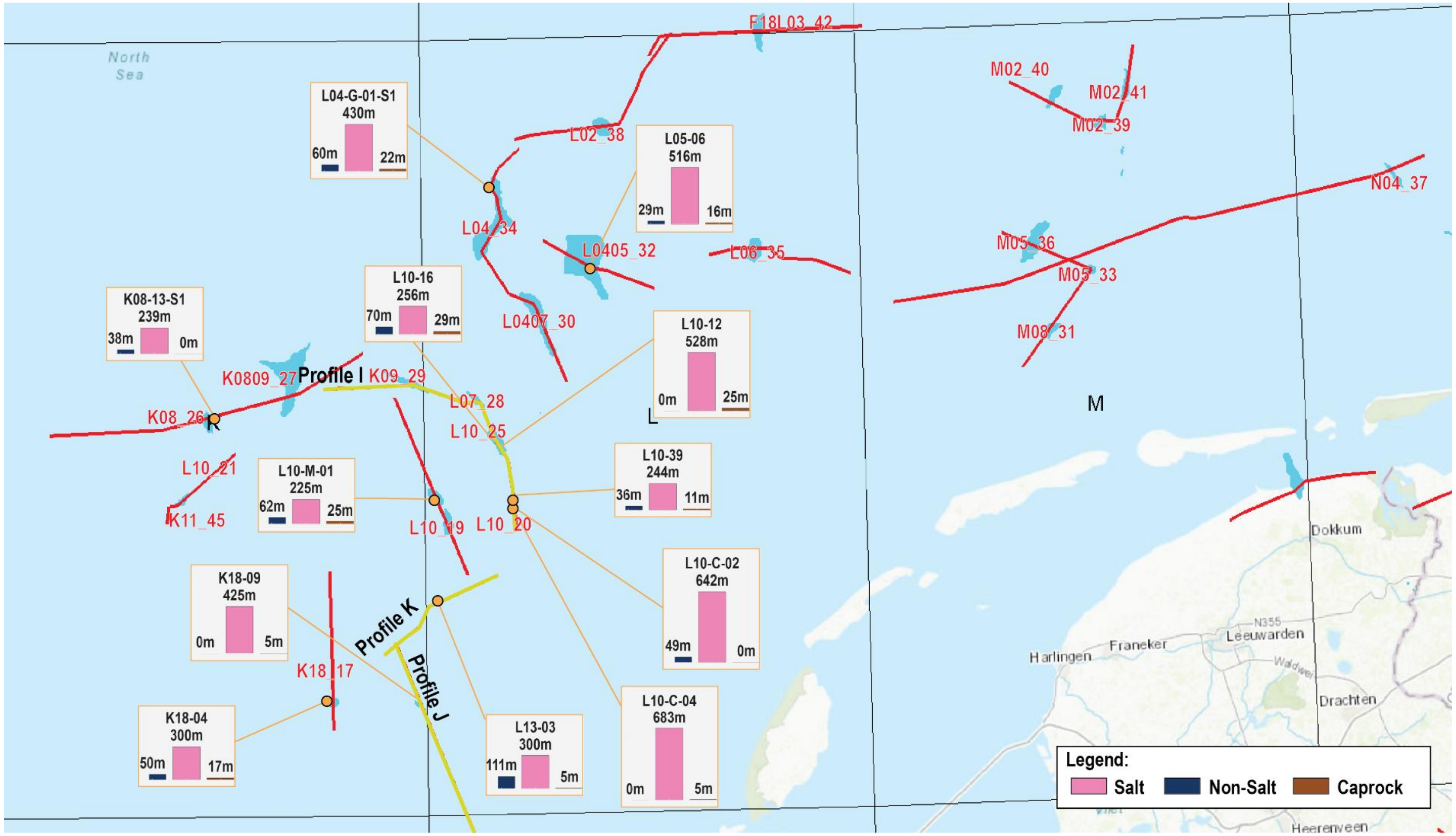

Figure 8. *Map of offshore Zechstein diapirs in the Dutch sector of the North Sea, showing cumulative thickness of Salt, Non-Salt, and Caprock lithologies above −1200 m depth. The map highlights extensive large shallow diapirs (tops at 600–1200 m) composed predominantly of halite, with thin caprocks (10–20 m). Yellow lines indicate the locations of seismic profiles I–K shown in Figure 9.*

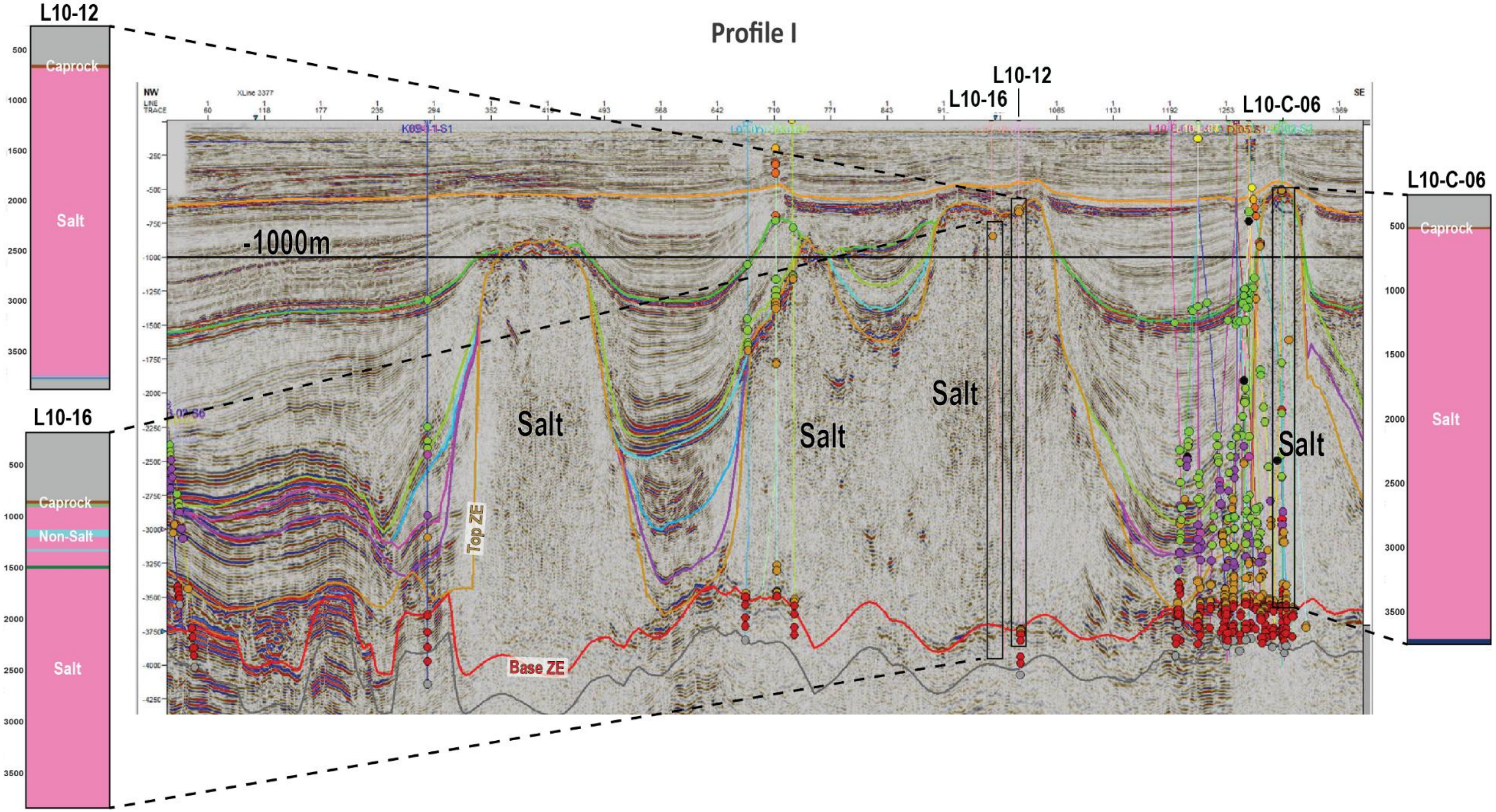
Profile I
L10-12
L10-16
L10-C-06
Caprock
Salt
Non-Salt
-1000m
Top ZE
Base ZE
NW
SE

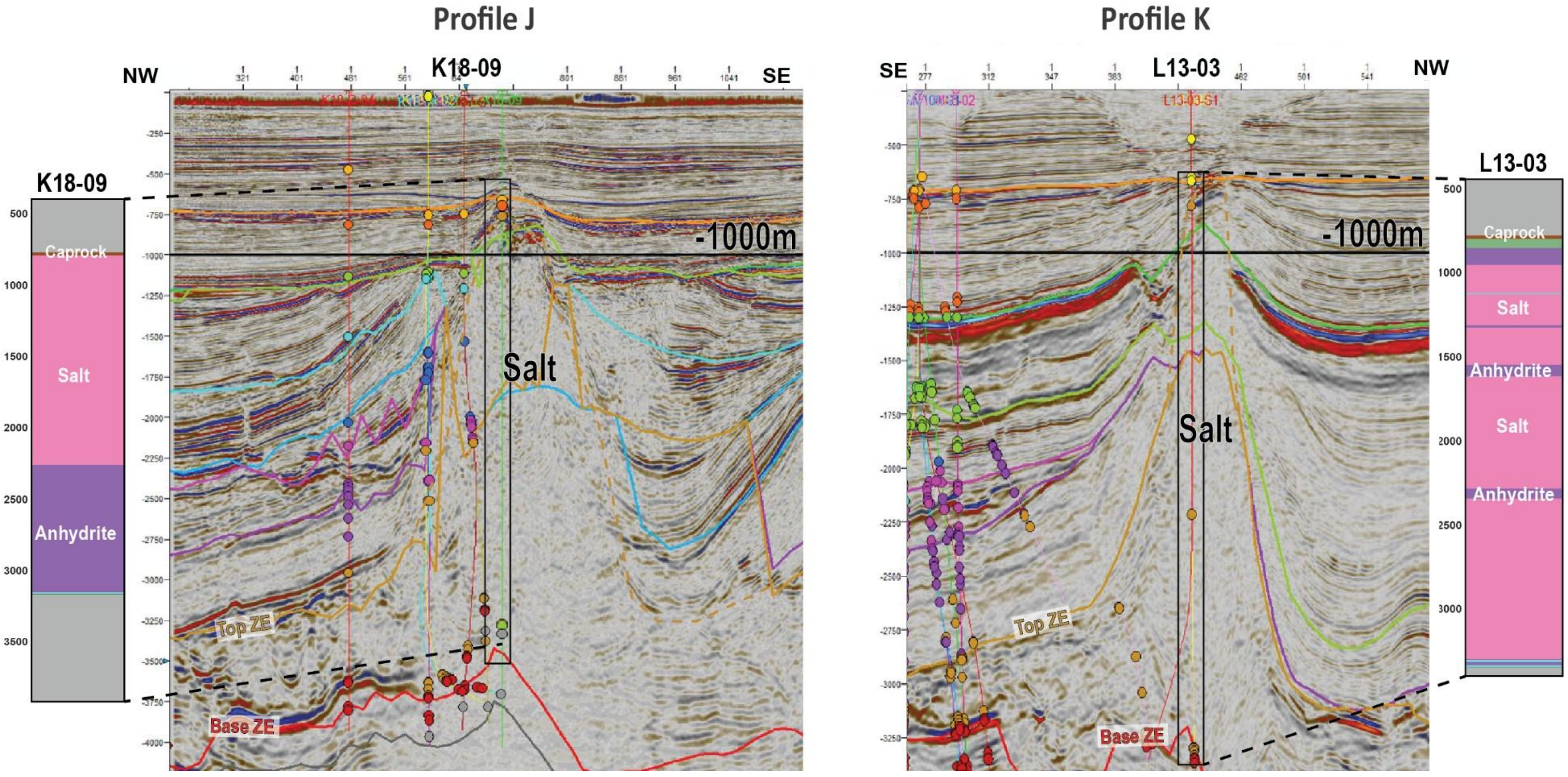

Figure 9. *Seismic profiles I–K across representative offshore Zechstein diapirs, including wells K18-09, L13-03, L10-C, L10-12, and L10-16. The sections reveal thick halite cores with minor anhydrite or carbonate intercalations concentrated near the tops of diapirs. Caprocks are typically thin (5–25 m), and overall structural deformation is limited, suggesting reduced hydrodynamic activity relative to onshore diapirs. It is to be noted that the seismic horizon interpretation does not correlate with wells K18-09 and L13-03, where the actual top of the diapir is positioned higher than the interpreted horizon. Our interpretation of the top Zechstein is marked with dashed lines.*

2. Detailed mapping of shallow salt domes and salt thickness distribution

2.1. Objectives

Building on the inventory of non-salt intercalations within the domes, the analysis aims to enhance existing models of the upper Zechstein structures under the same depth and thickness criteria applied previously.

2.2. Output

Updated maps of cumulative salt and non-salt thicknesses within the Zechstein layer, as files suitable for direct integration into Petrel™, TemisFlow™, and GIS software (Appendix 2).

2.3. Methodology

Starting from the TNO DGM Diep v5.0 model, lithological and stratigraphic descriptions were used to distinguish salt from non-salt lithologies, allowing non-salt intercalations—such as anhydrite, carbonate, shale and sandstone—to be isolated and mapped within the Zechstein interval. These descriptions were not newly interpreted from well logs but extracted from the model, and subsequently corrected during a lithological classification step to represent intra-salt heterogeneity accurately. Many wells required a reinterpretation by a more detailed analysis of original data in terms of composite well logs or lithological descriptions.

The updated cumulative thickness maps were constructed using wells where the total Zechstein interval is clearly defined (complete Zechstein series and well-log data), ensuring that only representative and reliable measurements were included. Previously applied corrections from the well classification process were incorporated and additional adjustments were made for wells exhibiting local mismatches or misalignments with existing seismic data. Wells lacking intra-salt lithological information or showing unreliable data were excluded to avoid introducing uncertainty into the model.

The resulting dataset comprises approximately 1,990 corrected well points, which were used to generate cumulative thickness maps for both salt and non-salt lithologies in XYZ point files, aligned with broader regional Zechstein trends. These maps represent total accumulated intervals rather than consecutive sub-units, providing a consistent, first-order geological framework for isolating and characterizing salt versus non-salt domains within the Zechstein formations of the Netherlands

Figure 12 further validates the refined thickness model by correlating cumulative salt, non-salt, and total Zechstein thicknesses with seismic profiles and corrected well data. The seismic section demonstrates strong agreement between the updated model and observed stratigraphy, confirming that the corrections applied to well tops and intra-salt intercalations improve the overall accuracy of the Zechstein geometry. Notably, the corrected well data reveal slightly higher total thicknesses than in the previous model, capturing intra-salt intercalations that were previously misrepresented.

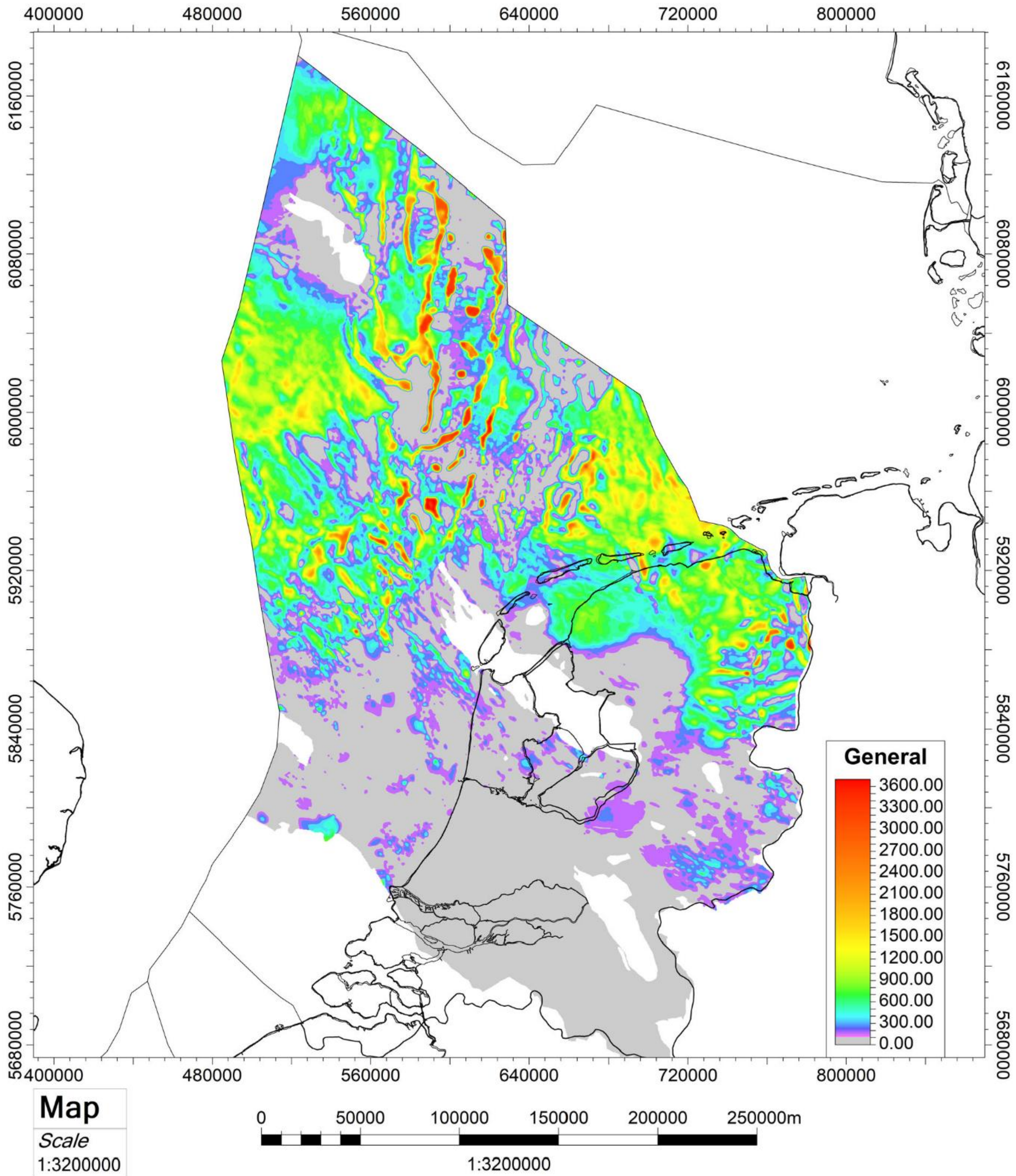

Figure 10. *Total Zechstein Salt Thickness Map. Cumulative thickness of Zechstein salt intervals (wells >100 m total salt thickness), displayed as color-contours and aligned with regional structural trends. The grey zone highlights areas where the salt thickness ranges from 0 to 100 m. The map highlights the spatial distribution and variability of salt accumulation across the Netherlands, showing the thickest sequences in the offshore and northern onshore domains and progressively thinner intervals toward the east and south. The major Zechstein salt structures are concentrated in the northern part of the Netherlands.*

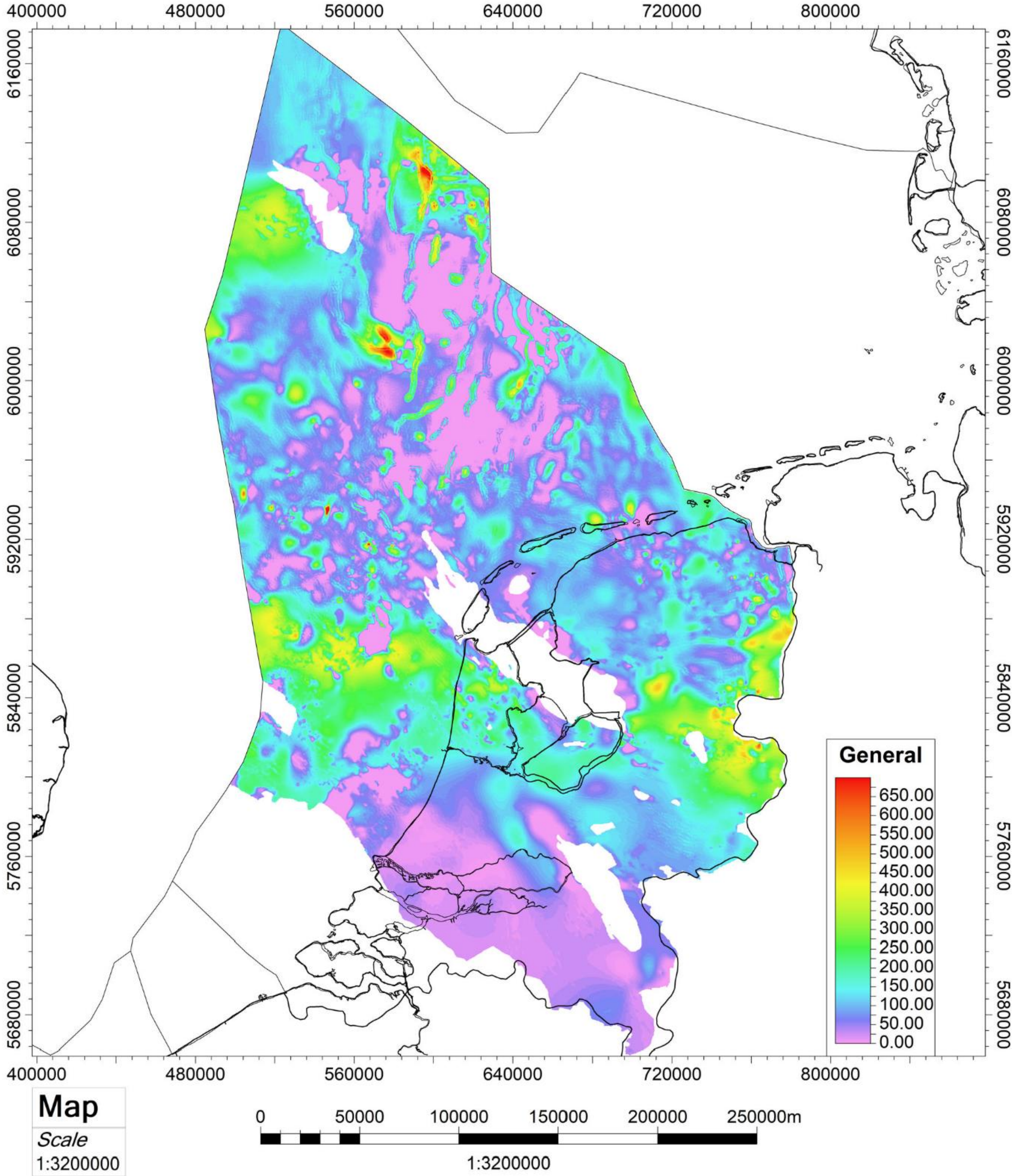

Figure 11. *Total Non-Salt Thickness Map. Distribution and cumulative thickness of non-salt intercalations (anhydrite, carbonate, and claystone) within the Zechstein Group layer. The map illustrates areas of increased lithological heterogeneity, with the most pronounced non-salt accumulations in the eastern and southern regions, reflecting greater structural complexity and reduced salt purity.*

2.4. Results

The updated Zechstein thickness maps reveal clear regional patterns in both salt and non-salt lithologies across the Netherlands. The total salt thickness map (Figure 10) shows the thickest Zechstein salt concentrated in the northern onshore and north western offshore regions, corresponding to the major salt structures, while salt is virtually absent in the southern Netherlands where the Zechstein is largely composed of non-salt lithologies. In contrast, the total non-salt thickness map (Figure 11) highlights areas where the Zechstein is thick but predominantly composed of intercalated lithologies such as carbonates, clay and anhydrite. This is particularly evident in the onshore domain, where the green colors indicate substantial non-salt intervals within otherwise thick Zechstein sections, emphasizing lithological heterogeneity that is not apparent on the salt map. The non-salt map therefore provides complementary information, distinguishing zones of thick but impure Zechstein from the more salt-dominated offshore and northern onshore diapirs.

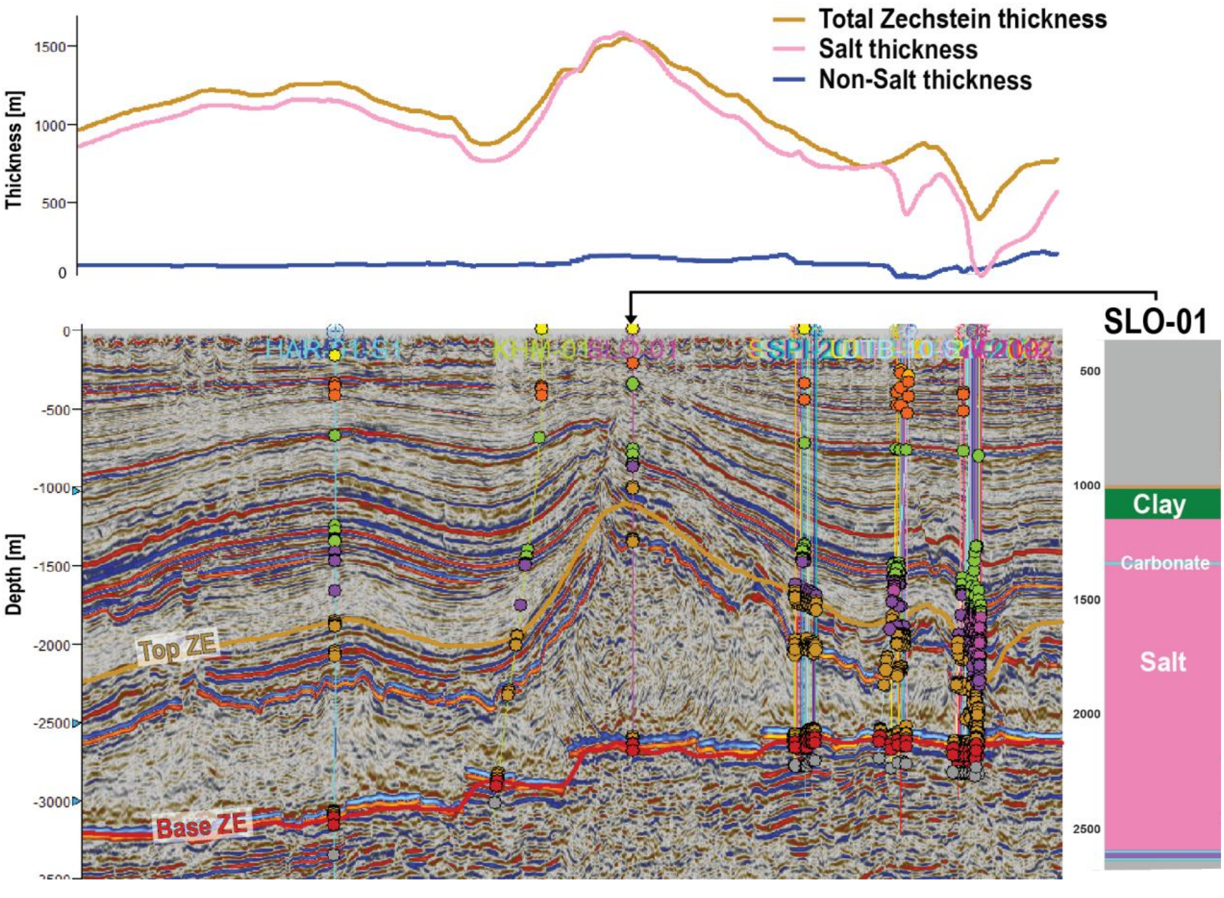

Figure 12. Correlation of updated Salt and Non-Salt thickness with seismic and well data. The top panel shows cumulative Salt and Non-Salt thickness derived from the updated model, while the bottom panel compares these thicknesses with seismic profiles and well data, including the top and base of the Zechstein interval. The comparison demonstrates consistency between the model and observations, highlights the improved distinction between Salt and Non-Salt layers, and shows better correlation with well data (e.g., SLO-01).

3. Summary of Lithological analysis

The resulting lithological dataset from section 1 and 2 is summarized in Figure 13. The Zechstein salt diapirs across the Netherlands display significant regional variability in thickness, composition and caprock development (Fig. 13). Offshore diapirs are the thickest, with salt sequences ranging from 500 to over 1200 m, largely pure with less non-salt intercalations and relatively thin caprocks of 10–20 m. Northern onshore diapirs are slightly thinner but still substantial, exceeding 2000 m in thickness in some locations, with caprocks varying between 5 and 80 m and generally composed of anhydrite, carbonate and claystone. Non-salt intercalations within the salt are limited, though lateral variability in caprock thickness is high, particularly at the crests of diapirs, indicating localized subrosion enhancement. Eastern onshore salt structures are smaller, generally less than 400 m thick, with frequent non-salt intercalations including anhydrite, carbonate and minor claystone and caprocks averaging 10–30 m, reflecting greater lithological heterogeneity and structural influence from faults. In the southern Netherlands, the Zechstein is thin (<80 m), largely dominated by carbonates with minor clay or salt and shows little evidence of diapirism or thick caprock development.

Figure 14 suggests that shallower diapirs generally have thicker caprocks, particularly those with tops within the Upper North Sea Group, whereas deeper diapirs, especially offshore, exhibit thinner caprocks. Shallow diapirs in onshore areas are influenced by active freshwater aquifers, which enhance local hydrodynamics and promote localized subrosion, while simultaneously supporting thicker caprock formation through precipitation of non-soluble minerals. In contrast, deeper diapirs experience limited interaction with shallow freshwater, resulting in thinner caprocks. These observations indicate that subrosion processes are the main driver of caprock variability, suggesting that dissolution occurs primarily in shallow Cenozoic sediments and that shallow diapirs are more susceptible to subrosion. However, thicker caprocks can also provide enhanced protection against erosion and dissolution, whereas thinner or heterogeneous caprocks increase vulnerability, particularly where faults or other heterogeneities are present near the salt structure.

The observed relationship between diapir depth, caprock thickness and subrosion intensity, together with the influence of aquifer salinity, underlines the need to better understand the coupled hydrodynamic and geochemical mechanisms driving these interactions. To address this issue, the following section presents modelling results that quantify the role of caprock properties and fluid salinity in controlling subrosion and salt dissolution.

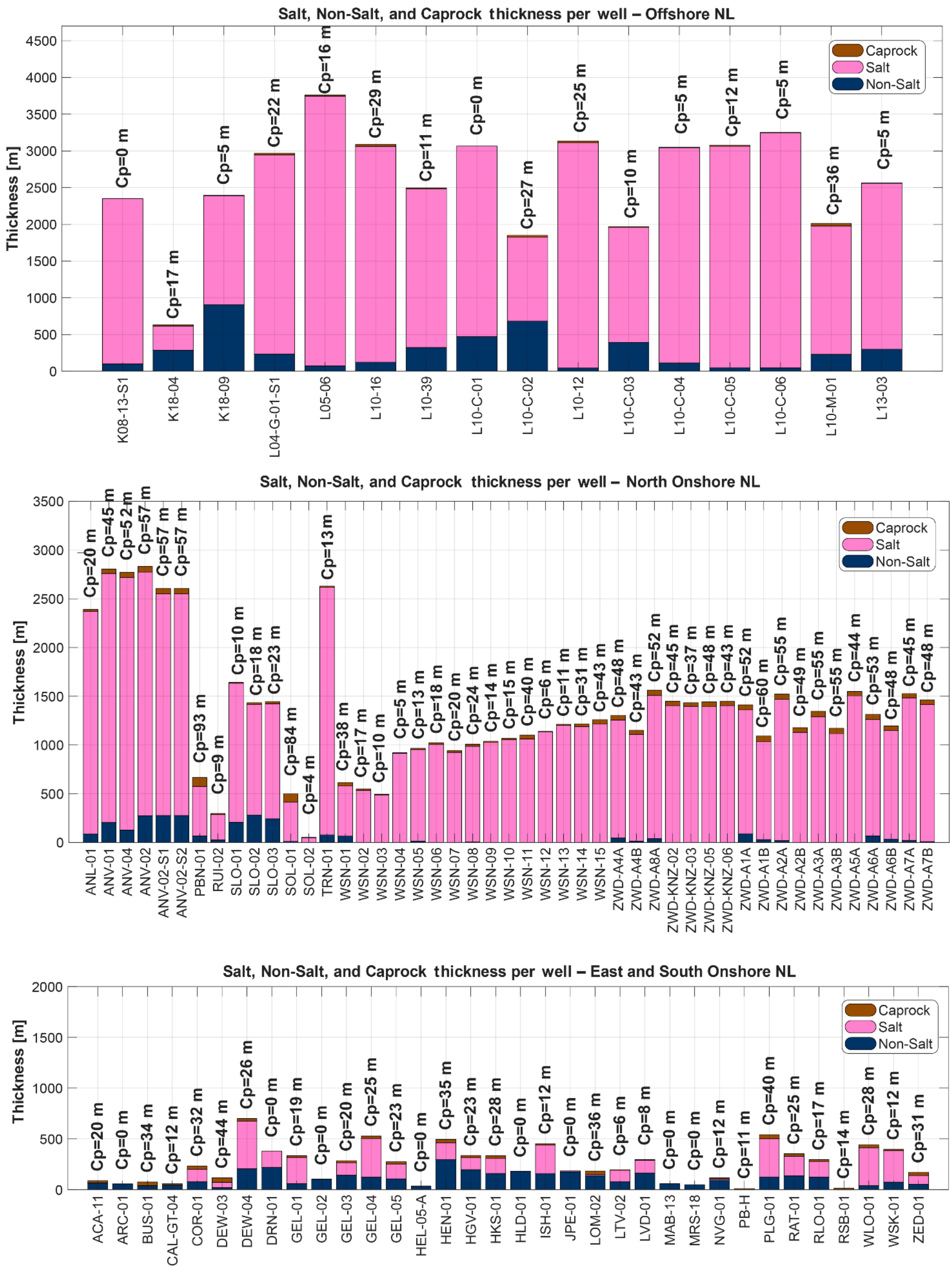

Figure 13. *Salt, Non-Salt, and Caprock thickness per Offshore well (top), Onshore Northern Netherlands (center), and Onshore Eastern and Southern Netherlands (bottom). Each bar represents the cumulative thickness within the Zechstein interval for individual wells. Caprock thickness values are indicated above each bar as Cp. This visualization highlights the regional variations in Zechstein composition, showing the greatest total thicknesses in the offshore domain and the thinnest sequences in the south-eastern Netherlands, where non-salt lithologies dominate.*

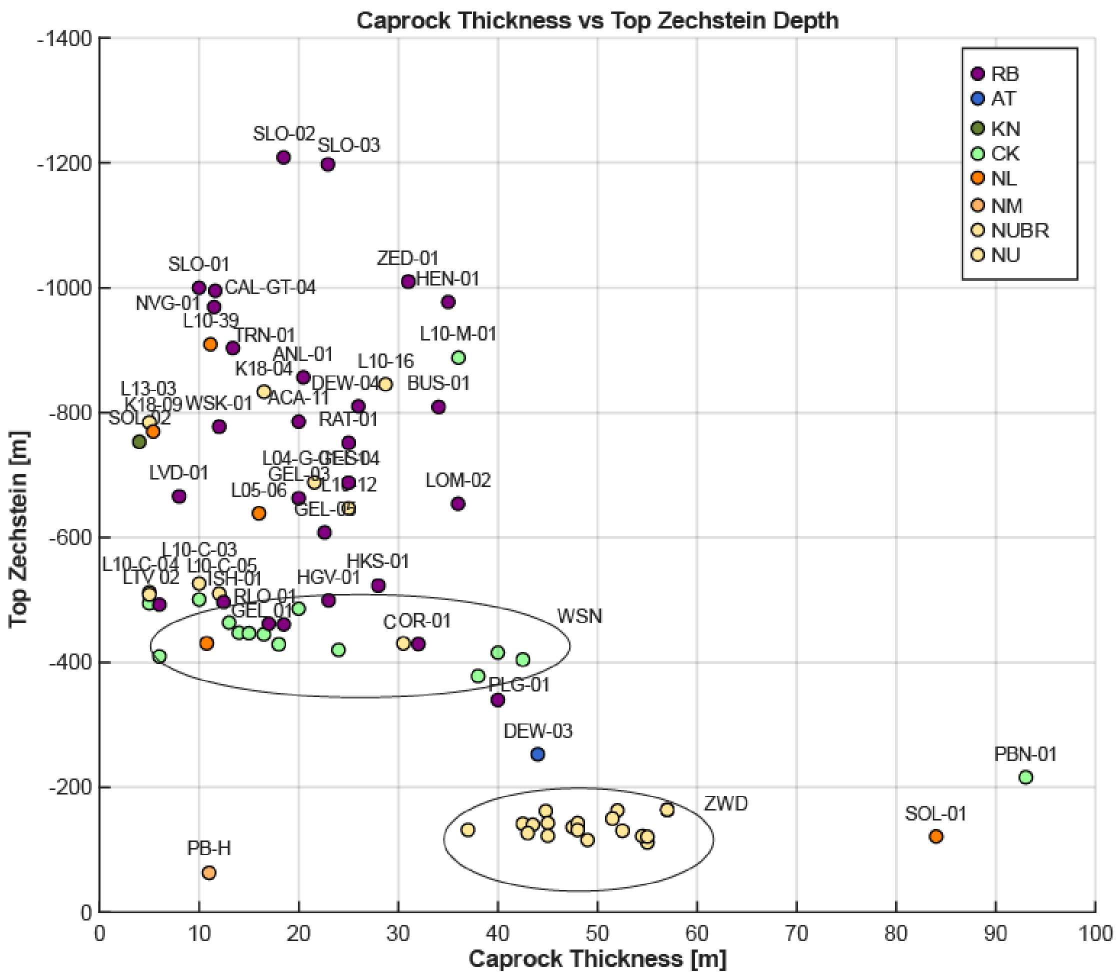

Figure 14*. The figure shows the depth of the Top Zechstein (Y-axis, inverted with 0 m at the top) and the Caprock thickness (X-axis) for both onshore and offshore wells. Each point represents a well, with colors indicating the lithology directly above the Zechstein (top lithology). NU – Upper North Sea Group, NUBR – Breda Formation, NM – Middle North Sea Group, NL – Lower North Sea Group, S – Upper Jurassic, RN – Upper Germanic Trias Group, RB – Lower Germanic Trias Group, CK – Chalk Formation, KN – Kimmeridgian/Cretaceous, AT – Altena Formation. The distribution shows that shallower salt structure tend to have thicker, more variable caprocks, while deeper structures generally show thinner, more uniform caps.*

4. Numerical Model

4.1 Governing equations

The present study employs the TemisFlow™ simulator to investigate the transport and dissolution of salt in groundwater systems at the basin scale in the northern Netherlands. A three-dimensional geological model was constructed by integrating depth maps, lithological distributions, hydrogeological properties, and geochemical and thermal datasets, including present-day and paleo-bathymetry information. TemisFlow™, in combination with the Arctem® calculator allows the coupled simulation of fluid flow and geochemical processes, explicitly accounting for salinity, density-driven migration, pressure-driven transport and NaCl concentration evolution. This software dynamically computes how saline plumes evolve over geological time, including salt dissolution and redistribution, providing a quantitative time-resolved representation of subsurface hydrogeochemical dynamics. The application of this workflow to a real dataset from the northern Netherlands provides a practical example, illustrating the importance of basin-scale-coupled-multiphysics simulations to quantify the impact of basin evolution on present-day NaCl concentrations.

Porosity in the model is depth-dependant following a Porosity-Effective Stress curve when fluid flow simulation is implemented. The effective stress σ is defined as the difference between the lithostatic stress SG, (i.e., the weight of the sediments) and the pore pressure P:

$$\sigma = SG\ \ P \quad (1)$$

The porosity-effective stress curve is defined by the following function:

$$\Phi(\sigma) = \Phi_1 + \Phi_a e^{-\frac{\sigma}{\sigma_a}} + \Phi_b e^{-\frac{\sigma}{\sigma_b}} \quad (2)$$

where, Φ_1 is the minimum porosity as defined in the porosity-depth law, Φ_a is the first porosity coefficient, Φ_b is the second porosity coefficient, σ_a is the first exponential factor of effective stress, σ_b is the second exponential factor of effective stress.

Permeability evolution was estimated using the Kozeny–Carman relationship, anchored at the porosity Φ:

$$\text{When } \Phi > 0.1\text{: } K = \frac{0.2\Phi^3}{S_0^2(1-\Phi)^2}\text{;} \qquad \text{When } \Phi < 0.1\text{: } K = \frac{\Phi^3}{S_0^2(1-\Phi)^2} \quad (3)$$

Where, K is the lithology intrinsic permeability (in m^2), S_0 is the specific area (in m^2/m^3). This approach ensures that the permeability decreases consistently with compaction while matching the prescribed surface value.

Fluid flow in the model is driven by pressure gradients imposed at the boundaries, following Darcy's law:

$$q=-\frac{k}{\mu}\nabla P \quad (4)$$

where q is the Darcy flux, k is the permeability, and μ is the fluid viscosity, which the model computes as a depth-dependent property of water, and ∇P is the pressure gradient. The flow is further influenced by salinity-dependent density variations, which modify the effective driving force:

$$\nabla P_{\text{eff}}=\nabla P+\rho g\nabla z \quad (5)$$

where ρ is the fluid density, g the gravitational acceleration and z the vertical coordinate. Fluids migrate from high to low pressure zones, with denser saline water tending to sink and less saline water rising.

Salt transport in groundwater is modelled using the coupled advection-dispersion equation, which accounts for both transport with flowing water and spreading due to molecular diffusion and mechanical dispersion. Dissolution of salt occurs when the aqueous phase is undersaturated relative to the salt solubility, $C_{w,\text{sat}}$ which depends on temperature, pressure, and water chemistry. This process is represented as a source term that drives the local salt concentration toward equilibrium

$$r_w=\frac{\partial}{\partial t}\Big(\big(C_{w,\text{sat}}-C_w\big)\rho_w\Big) \quad (6)$$

where C_w is the current concentration of salt in water, and $C_{w,\text{sat}}$ is the equilibrium solubility under the prevailing temperature, pressure, and chemical conditions. *Pw* is the density of water.

Once dissolved, salt spreads in the groundwater through molecular diffusion, where ions move from regions of high concentration to low concentration, and through mechanical dispersion, which arises from flow heterogeneity in the porous medium and pore-scale velocity variations. The combined effect of dissolution, diffusion, and dispersion is captured in the transport coefficient Λ_w

$$\Lambda_w=\rho_w s_w\phi\left(\frac{D_{w,\text{diff}}\alpha(T)}{\tau}+D_{w,\text{disp}}|U_w|\right) \quad (7)$$

where $D_{w,\text{diff}}$ is the molecular diffusivity of salt, $D_{w,\text{disp}}$ the hydrodynamic dispersion coefficient, τ the rock tortuosity set to 2, α(T) a temperature-dependent viscosity correction, and U_w the Darcy velocity of water. $\rho_w s_w\phi$ scales the molecular diffusion term to bulk porous medium. This framework ensures that the evolution of salt concentration in groundwater reflects both thermodynamic equilibrium constraints and spreading due to physical transport processes.

4.2. Strategy

To optimally constrain the model, we first built a conceptual model to test the sensitivity of subrosion to the main parameters the flow rate, salinity and caprock porosity. This allowed us to isolate the role of each component in controlling subrosion processes. In a second stage, we applied a real-case scenario model with a more realistic, data-based parameterization to simulate subrosion rates and the evolution of salt structures in the Northern Netherlands. The results were subsequently correlated with real-world data to validate the model, and constrain the most realistic parameter ranges governing subrosion in the Northern Netherlands.

5. Conceptual diapir-scale scenario model

5.1 Objectives

The conceptual model aims to test different parameters and processes to estimate the range of subrosion rates and isolate the effects of fluid flow, salinity and caprock porosity, in order to better understand diapir subrosion and inform the real-case scenario model.

5.2 Output

Formulations and solutions to estimate subrosion rates for a simple diapir as a function of fluid flow and caprock properties (equation 8 and 9)

5.3 Modelling approach

A conceptual 3D model domain measuring 20 km × 20 km × 4 km (Fig. 15) was developed to represent a generic salt diapir intersecting a sandy aquifer confined between two sealing layers. The model is used to test the influence of fluid salinity and caprock properties on subrosion processes by varying flow rate, caprock thickness, porosity and fluid salinity (Table 3). This approach allows evaluation of the relative importance of each parameter in controlling dissolution dynamics, using an improved setup that explicitly accounts for the presence and properties of the caprock.

5.4 Results

The conceptual 3D model examines how fluid flow rates and caprock porosity control diapir subrosion. Fluid flow simulations show that velocities are highest near the diapir crest, where the combination of enhanced permeability and local pressure gradients drives upward-directed flow and promotes localized dissolution of the salt (Fig. 15). For diapirs without a caprock, subrosion rates are strongly influenced by the flow velocity and to a lesser degree the salinity of the overlying aquifer. Low-salinity water and higher velocities lead to significantly greater dissolution with values ranging from 40 to 170 m/Myr (Fig. 16a). However, the salinity plays a limited role as it only slightly reduces the subrosion rate of 10-15 m/Myr.

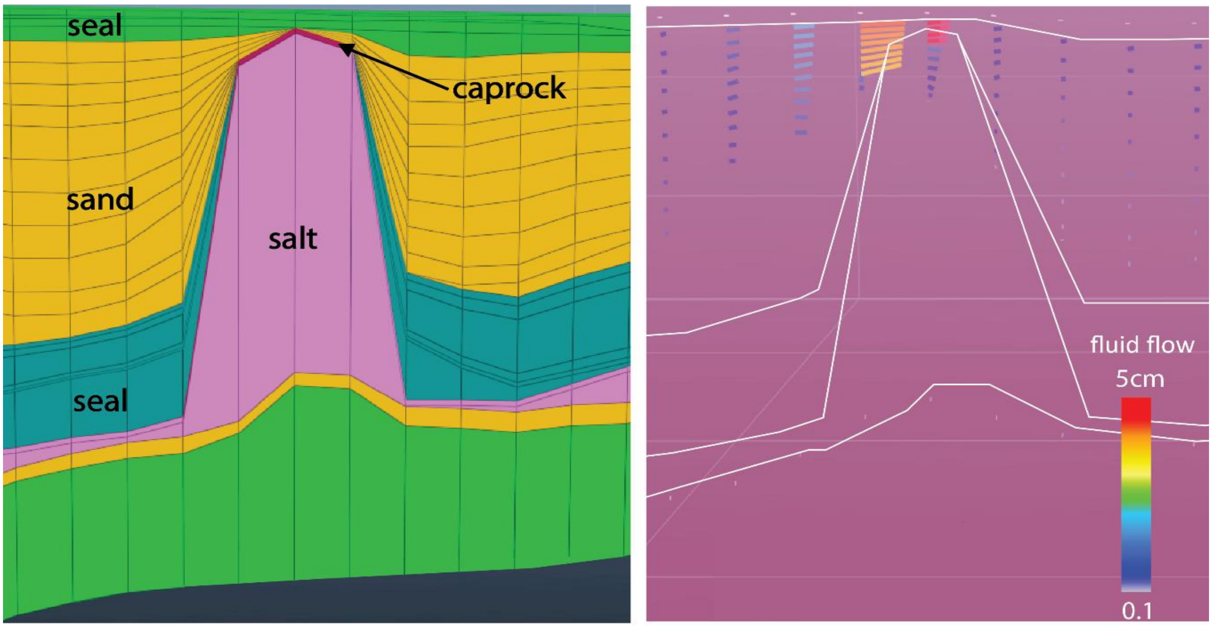

Figure 15. *2D section of the 3D conceptual model setup and flow field representation. Left panel: lithological layering illustrating the model configuration, where a salt diapir with an overlying caprock intersects a sandy confined aquifer. Right panel: velocity vector field showing fluid flow around the diapir; the highest velocities occur near the diapir crest, where enhanced permeability and pressure gradients induce upward-directed flow.*

Simulation	**Caprock thickness m**	**Caprock porosity (θ)**	**τ tortuosity**	**Dissolution rate m/Myr**	**Mean flow velocity m/yr**
θ = 2%. High tortuosity	40	0.02	3	8.43E-04	1.42
θ = 2%. Thick caprock 60m	60	0.02	2	6.00E-02	1.42
θ = 2%. Low velocity	40	0.02	2	8.92E-02	0.153
θ = 2%. Low permeability	40	0.02	2	8.94E-02	1.75
θ = 2% medium velocity	40	0.02	2	9.18E-02	1.43
θ = 2%. High velocity	40	0.02	2	9.12E-02	5.65
θ = 2%. Thin caprock 15m	15	0.02	2	2.35E-01	1.43
θ = 10%. High tortuosity	40	0.1	3	3.64E-01	1.43
θ = 10%. Low velocity	40	0.1	2	2.24E+00	0.418
θ = 10% medium velocity	40	0.1	2	2.38E+00	1.44
θ = 10% high velocity	40	0.1	2	2.42E+00	6
no caprock very low velocity	0	salt	2	4.39E+01	0.213
no caprock low velocity	0	salt	2	4.97E+01	0.77
no caprock	0	salt	2	1.15E+02	2.06
no caprock high velocity	0	salt	2	1.44E+02	5.58

no caprock very high velocity	0	salt	2	1.69E+02	13.52
no caprock influx salinity 5g/l	0	salt	2	9.99E+01	2.10
no caprock influx salinity 5g/l	0	salt	2	1.30E+02	5.65
no caprock influx salinity 100g/l	0	salt	2	9.56E+01	2.10
no caprock influx salinity 100g/l	0	salt	2	1.25E+02	5.65

Table *3*. Summary of conceptual model parameters and results. The table lists all simulation scenarios, including presence or absence of caprock, caprock thickness, porosity, fluid flow velocity and salinity of the overlying aquifer, along with the resulting subrosion rates. θ = *porosity and the mean fluid flow velocity is fluid flow velocity at the crest of the diapir exclude the caprock.*

For a simple set-up, fresh water and pure halite we propose a logarithmic relationship between fluid flow and subrosion rate (expressed in dissolved thickness in m/Myr):

$$h = 33.15 \ln(v) + 82.85 \quad (8)$$

Where h = subrosion rate (m/Myr) and v is the average flow velocity in the overlying aquifer at the crest of the diapir in m/year

The presence of a caprock considerably alters the dissolution dynamics. Simulations show that even relatively thin caprocks reduce subrosion rates significantly (10 – 250 cm/Myr) and the rate of salt loss becomes largely controlled by intrinsic caprock properties, including porosity, thickness and fluid salinity, rather than by flow velocity (Fig. 16, bottom panel). If the fluid flow is not a controlling factor and can be nullified, the subrosion rate can be estimate with a diffusion controlled analytical formulation

$$h = \frac{C_{\mathrm{salt}} - C_{\mathrm{fluid}}}{E} \cdot K \cdot \phi^{\tau} \quad (9)$$

where h is the subrosion rate (m/Myr), C_{salt}=0.35 is the salt concentration fraction in Kg/L, C_{fluid} is the concentration in salt (NaCl) in the fluid in Kg/L, E is the caprock thickness in m, ϕ caprock porosity, τ= 2 is the tortuosity and K= 23147.38 is a scaling factor to convert units and account for molecular properties.

The comparison of simulated subrosion with a diffusion-controlled analytical formulation further confirms this behaviour: the affine correlation demonstrates that, for capped diapirs, subrosion is primarily diffusion-limited through the caprock and is less sensitive to variations in fluid flow (Fig. 17). These results emphasize that the presence and characteristics of the caprock are the main factors controlling the stability of salt diapirs under hydrogeological forcing. High porosity or thinner caprocks increase vulnerability to dissolution, whereas thicker or low-porosity caprocks provide effective protection. The conceptual model therefore provides a robust framework to isolate the influence of individual parameters—flow, salinity and caprock properties—and supports the parameterization of the real-case, basin-scale model for the northern Netherlands. This understanding is essential for predicting the long-term evolution of Zechstein diapirs.

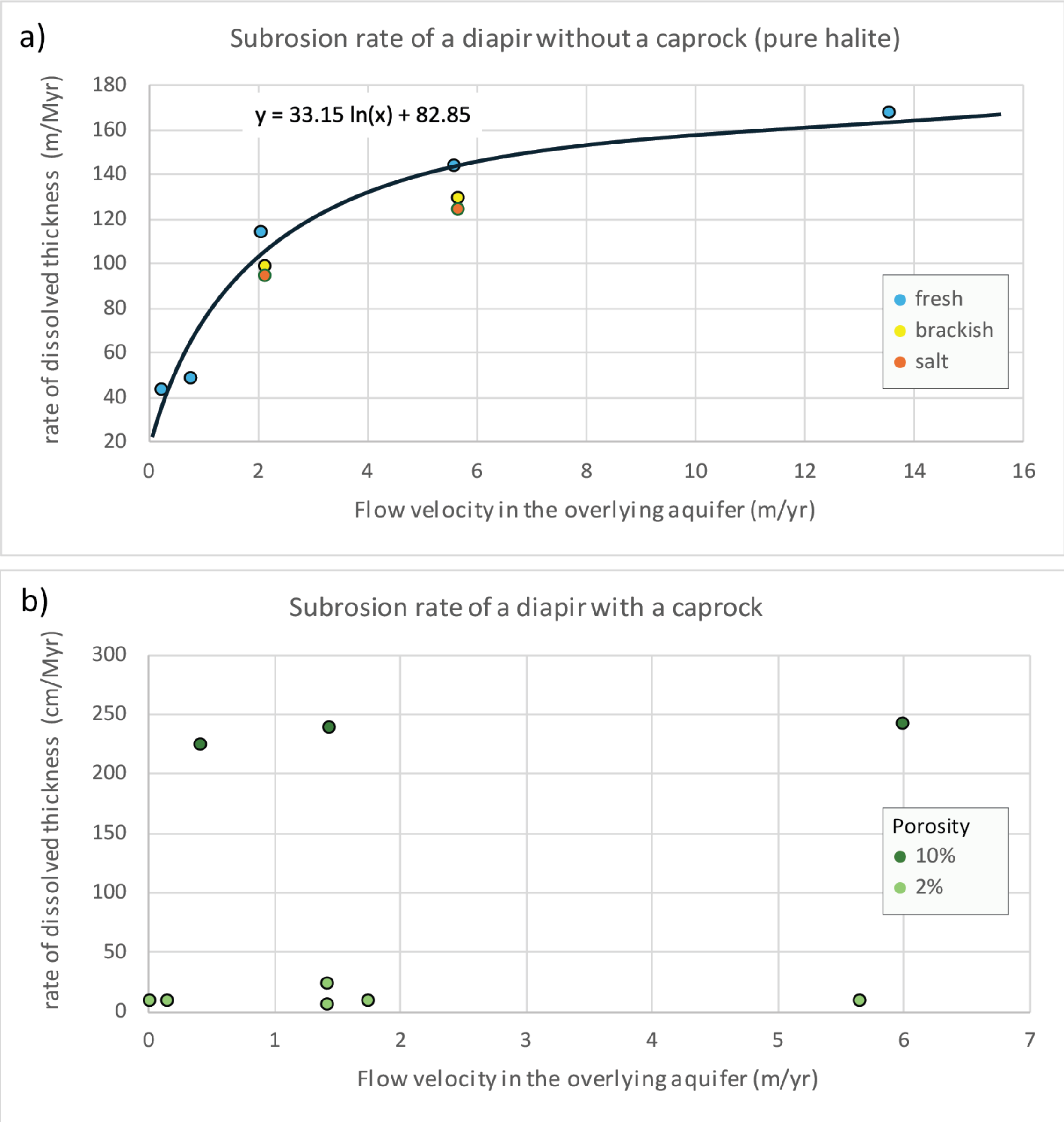

Figure 16. *Subrosion rate of the diapir, expressed as the rate of dissolved thickness vs flow velocity in the overlying aquifer. a) results for a diapir without caprock (pure halite) in m/ Myr under different water salinities ([NaCl] = 0; 1,000; 100,000 mg/L). b) results for a diapir overlain by a caprock, in cm/Myr, and tested under varying porosity conditions. Nearly constant subrosion rates suggest that, for diapirs with a caprock, flow rate has a limited impact on subrosion.*

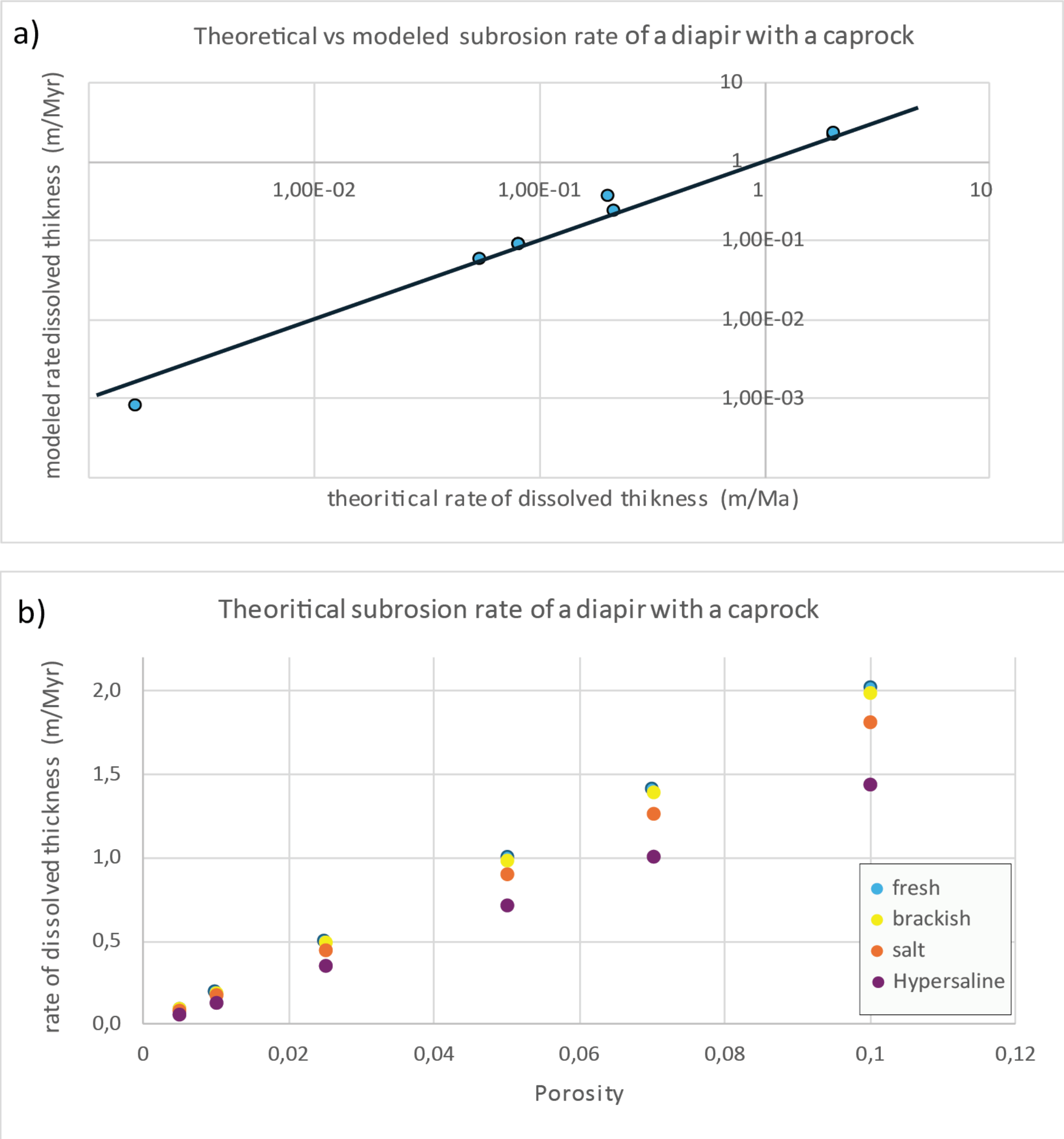

Figure 17. *a) Theoretical versus modelled subrosion rates for diapirs with a caprock, showing the fit between simulated results and the analytical formulation. The correlation follows an affine relationship, indicating a good fit between theoretical model and simulated one. b) Calculated theoretical subrosion rates as a function of porosity of caprock for different water salinities, representing freshwater, brackish, seawater, and hypersaline conditions ([NaCl] = 0, 1,000, 35,000, 100,000 mg/L), illustrating the increase of subrosion with porosity and the decrease with increasing salinity. The rate is primarily controlled by the caprock's porosity, salinity, and thickness, consistent with a diffusion-controlled dissolution formulation (equation 9).*

6. Real case Scenario basin scale model

6.1 Objectives

The objectives of the real-case basin-scale scenario model are to enhance the TemisFlow™ basin model of the Northern Netherlands, developed in the previous study (Li et al., 2024), by integrating hydrodynamic boundary conditions for fluid flow (including recorded permeability, porosity and pressures), incorporating geological parameters such as lithological corrections and caprock properties, and accounting for geochemical factors such as salinity. The model is intended to perform sensitivity analyses and simulate groundwater flow, salinity evolution and subrosion rates, providing a detailed mapping of dissolution processes within the study area.

6.2 Output

Past and present-day subrosion-rate maps in grid format, derived from new observation-based hydrodynamic and geological parameters. The updated TemisFlow™ model (Appendix 3).

6.3 Model approach

To generically quantify subrosion processes in different Dutch salt domes at various stages of evolution, a 3D model was previously constructed at the (sub-)basin scale, corresponding to the northern Netherlands onshore. The model domain encompasses the main diapiric Zechstein structures, covering approximately 100 km × 100 km across the Groningen, Friesland and Overijssel provinces. The model domain is described in Li et al (2024), but it is similar to the North-eastern zone delimited in Figure 1 (Area used for Fig. 2). The updated model integrates new hydrodynamic boundary conditions from the REGIS II national model and a salinity framework derived from the LHM Fresh-Salt model of the Netherlands Hydrological Instrument (NHI), while deeper levels are constrained using literature data (Table 4). Caprocks have been implemented manually on the major diapirs at depths above ~2000 m (Fig. 21). This phase of the study focuses on gathering and integrating all relevant data into the model to test subrosion processes under realistic geological and hydrodynamic conditions, providing a foundation for both regional assessments and site-specific analyses.

6.3.1 Geological and hydrodynamical parameters

The updated TemisFlow^{TM} model integrates improved boundary conditions for fluid flow and salinity, -i.e., the main controls on subrosion. The resulting set of data compiled from this integration is summarized in Table 4. Details on the parameterization and history of deeper formations are presented in the next section, based on literature to inform the geological and hydrodynamic framework.

Present-day fluid flow

Present-day fluid flow can be relatively well constrained using current data on hydraulic gradients and pressure distributions. The shallow subsurface is well characterized by national groundwater surveys (Stuyfzand, 1993; Broers et al., 2021) and hydrological models.

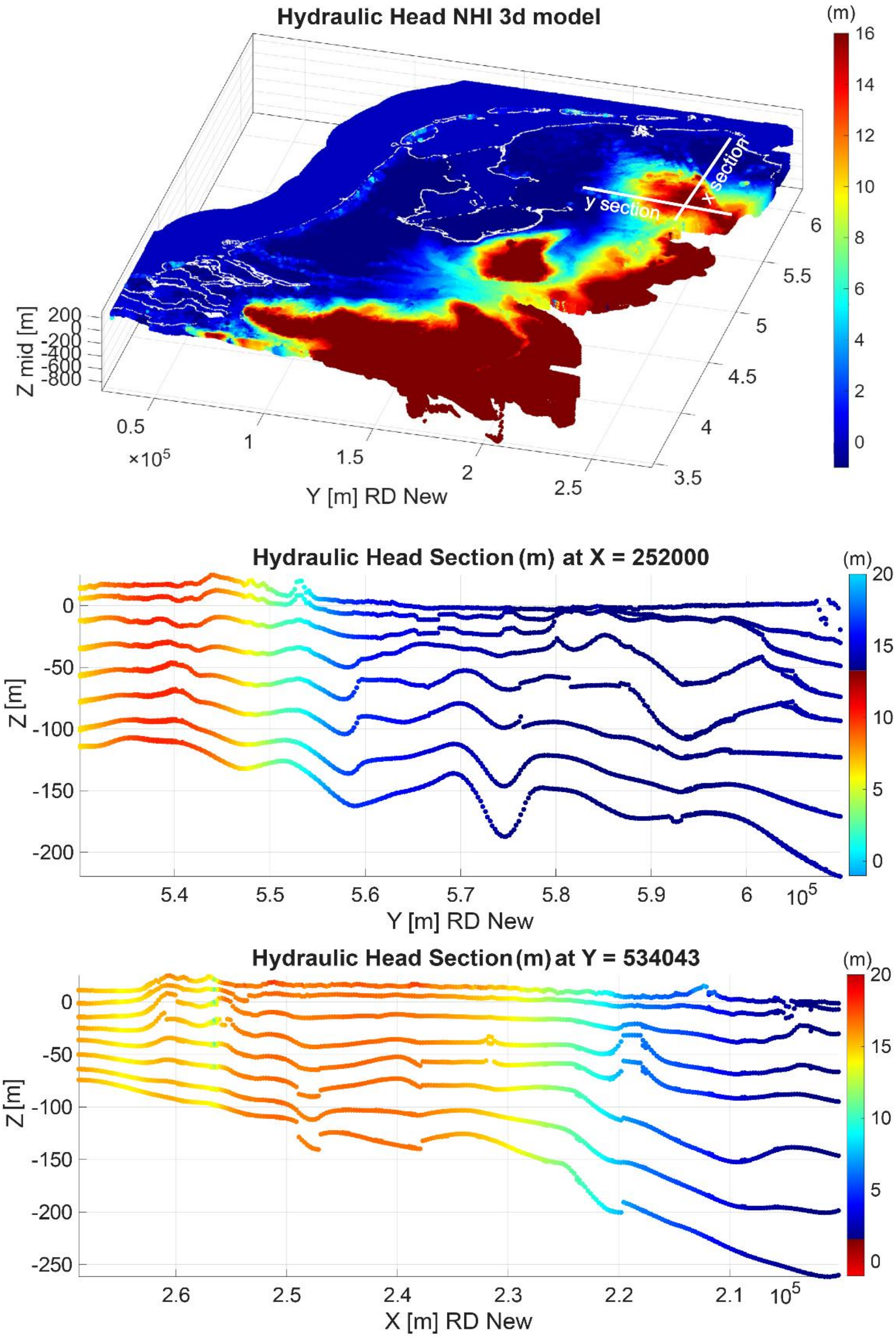

Figure 18: *Hydraulic head from the National 3D NHI Groundwater Model Workflow (Delsman et al., 2023). The top panel shows the 3D hydraulic head distribution over the Netherlands, with the X- and Y-sections highlighted by white lines. The middle panel shows the cross-sectional hydraulic head along the X-axis, and the bottom panel shows the cross-sectional hydraulic head along the Y-axis. Maximum hydraulic head values reach approximately 17 m, equivalent to 1.62 bar of pressure. A strong northward decrease in hydraulic head indicates a negative pressure gradient toward the north, driving groundwater flow. The coordinate reference system is the RD Netherlands, EPSG:28992.*

Aquifer parameters are available in the REGIS II hydrological model, which provides boundary conditions for our model inputs in table 4 (Hummelman et al., 2019). The hydraulic head data from the National 3D NHI Groundwater Model Workflow (Delsman et al., 2023) allow constraining the boundary pressure gradient that drive the fluid flow (Fig. 18).

In contrast, the deeper subsurface—from the Lower North Sea Group down to the Permian—lacks widespread direct measurements of fluid rates or hydraulic parameters. However, indirect methods can be used to estimate first-order values of fluid flow dynamics. In particular, permeability measurements from core data, overpressure and salinity data can serve as proxies for flow restrictions in each geological layer, indicating whether the system is hydraulically confined or semi-confined (Table 4).

Past fluid flow

In the north Netherlands, large-scale northward-flowing groundwater systems have been identified, originating at the southern and south-eastern margins during different geological periods within the shallow aquifer: Late Carboniferous–Early Permian, Jurassic–Early Cretaceous, Late Cretaceous, Oligocene and Holocene (Verweij, 1999; Lee et al., 1989). Analyses of diagenetic processes suggest that fluid–rock interactions were particularly intense during periods of subaerial exposure, when fresh water could efficiently recharge shallow aquifers (Ziegler, 2006). Geochemical data indicate that contamination by halite from salt diapirs was most pronounced during these recharge events (Glasbergen, 1981). During periods of active sediment deposition, aquifer salinity primarily reflects the depositional environment, which was mostly marine and was later diluted by incoming fresh water.

Overpressure

In fluid flow studies, overpressure is used as a proxy for controlling fluid flow in each layer. Overpressure is defined as the difference between measured pore pressure and hydrostatic pressure at a given depth (Verweij et al., 2025). It reflects both the potential energy driving water movement and the degree to which flow is restricted by overlying or surrounding layers. In unconfined aquifers, overpressure gradients relate primarily to variations in hydraulic head at the water table. In semi-confined aquifers, partial restriction by semi-permeable layers can create moderate overpressure when recharge exceeds leakage or pumping alters pressures. In confined aquifers, water trapped between impermeable strata can lead to significant overpressure caused by sediment compaction, geological compression, or tectonic stress, with wells often exhibiting artesian conditions.

The Cenozoic sediments (NU–NM–NL groups) are generally close to hydrostatic pressure (TNO & EBN SNS database, 2020). Only a few overpressured conditions are observed offshore, in mudstones of the Lower North Sea Group, due to rapid Late Cenozoic loading. In the Northern Onshore Netherlands, the Cenozoic aquifers support long-term fluid flow, with flux and direction largely controlled by permeability, hydraulic gradients and overburden. The Tertiary units are predominantly argillaceous, further influencing flow patterns (Japsen, 1999).

Env.	Formation / Group	Code	Lithology	Depth Range (m)	K_h (m/d) [*8]	K_v (m/d) [*8]	k (mD) [*9,10]	Overpressure (Bar) [*1,2,3]	Chloride (mg/L) [*4,5,6,7]
Continental	Boxtel	NUBX	Fine to coarse aeolian sand	0 – 30	3 – 10	-	-	Hydrostatic	10 – 50
	Drente + Eem + Kreftenheye	NUDR + NUEE + NUKR	Glaciolacustrine fine sand + clay	0 – 30	-	1e-3 – 5e-3	-	Hydrostatic	10 – 50
	Peelo + Urk + Drachten	NUPE + NUURTY + NUDN	Fine to coarse glacial sand + clay layers	0 – 200	1 – 25	1e-4 – 1e-2	-	Hydrostatic	10 – 50
	Urk	NUUR	Fine to coarse fluvial sand, sparse clay	10 – 90	10 – 40	-	-	Hydrostatic	10 – 50
	Appelscha	NUAP	Fine to coarse fluvial sand	50 – 120	20 – 90	-	-	Hydrostatic	10 – 50
	Peize + Waalre	NUPZ-WAz1-z2	Fluvial to deltaic sand	30 – 180	20 – 80	-	-	Hydrostatic	10 – 50
	Peize	NUPZc	Shallow marine fine sand and clay	50 – 255	1 – 10	1e-2 – 1e-1	-	Hydrostatic	10 – 50
	Peize + Waalre	NUPZ-WAz3	Fluvial to deltaic sand	50 – 280	5 – 50	-	-	Hydrostatic	10 – 50
subaerial exposure									
Marine	Oosterhout + Maassluis	NUOT + NUMS	Shallow marine fine sand and clay	100 – 375	2 – 10	3e-3 – 1e-2	-	Hydrostatic	80 – 500
	Breda	NUBR	Marine silty clay	125 – 450	1e-2	2e-3	-	Hydrostatic	1e3– 2e4
	Rupel + Tongeren	NMRU + NMTO	Marine clay	150 – 700	-	-	1e-4 – 1 e-3	0 – 5	3.3e3– 3e4
subaerial exposure									
Marine	Brussel	NLDOBR	Clayish sand	200 – 850	-	-	100 – 1000	0 – 5	1e4 – 7e4
	Dongen + Ypresian	NLDOIE	Marine clay	200 – 1,200	-	-	1e-4 – 1e-3	0 – 20	1e4– 7e4
subaerial exposure									
Marine	Chalk	CK	Chalk	600 – 2,000	-	-	5e-2 – 100	10 – 50	1e4 – 5e4
	Rijnland	KNGLU	Holland marl	1,000 – 2,200	-	-	1e-2 – 1	10 – 60	1e4 – 5e4
	Rijnland	KNNC	Marine silty claystone	1,000 – 2,200		1e-3 – 1e-1	4e4– 1.2e5	10 – 60	
Lacus.	Niedersachsen	SK	Silty claystone, marl and limestone	1,200 – 2,500	-	-	5e-2 – 50	10 – 60	
subaerial exposure									
Marine	Posidonia	ATPO	Posidonia marine shale	1,200 – 2,500	- -		1e-6 – 1e-5	10 – 60	4e4 – 1.2e5
Restricted-marine	Aalburf	ATAL	Fine-grained mudstones	1,200 – 2,500	- -		1e-6 – 1e-4	10 – 60	4e4 – 1.2e5
	Keuper	RNK	Dolomite, claystone, evaporite	1,500 – 2,700	- -		1e-2 – 10	10 – 120	4e4 – 1.2e5
	Muschelkalk	RNMU	Marl, evaporite, limestone	1,500 – 2,700	- -		1e-3 – 10	10 – 120	4e4 – 1.2e5
	Röt	RNROU	Rot silty claystone	1,600 – 2,800	- -		1e-3 – 1e-1	10 – 120	4e4 – 1.2e5
	Röt	RNRO	Rot evaporite (sabkha)	1,600 – 2,800	- -		~0	10 – 120	4e4 – 1.2e5
	Solling	RNSOC	Alternation sand, silt, clay	1,600 – 2,800	- -		1e-2 – 1e1	10 – 120	4e4 – 1.2e5
	Buntsandstein	RB	Clay, silt, sand	1,600 – 3,000	- -		1e-2 – 1e1	10 – 120	4e4 – 1.2e5
	Zechstein Caprock	ZECP	Anhydrite, gypsum, clay	1,600 – 3,400	- -		~0	10 – 120	4e4 – 1.2e5
	Zechstein salt	ZE	Zechstein salt	1,600 – 3,400	- -		~0	10 – 120	4e4 – 1.2e5
	Rotliegend	RO	-	2,000 – 3,900	- -		0 – 1000	10 – 120	4e4 – 1.2e5
subaerial exposure									
Mixed	Carboniferous	PreRO	Silty to sandy mudstone/limestone	2,200 – 4,400	- -		0 – 10	10 – 50	4e4 – 1,2e5

Table 4. *Summary of geological and hydrodynamic data for major aquifers and formations in the northern Netherlands. Both continental (Quaternary) and deeper marine and subaerial-exposed formations are included, highlighting variations in fluid flow properties and salinity across depositional environments and stratigraphic units. The table compiles data from hydrological models (REGIS II; Hummelman et al., 2019) and literature sources. Kh, Kv, k are the horizontal, vertical hydraulic conductivity and permeability, respectively. Overpressures, salinity and permeability values are compiled from literature and model data:*

- Overpressures: [1] Verweij, 2003; [2] Verweij et al., 2011; [3] Verweij et al., 2012; [4] TNO, 2015; [5] TNO & EBN, 2020.

- Salinity (Cl^- concentrations): [4] Delsman, et al. 2023; [5] Broers et al., 2021; [6] Glasbergen, 1981; [7] Hummelman et al., 2019.

- Hydraulic conductivity / Permeability (K_h, K_v, k): [8] Hummelman et al., 2019 (REGIS II); [9] Stuyfzand, 1993; [10] Broers et al., 2021.

There is no consensus on whether the Cretaceous Chalk acts as an aquifer or an aquitard (Verweij, 2003). Overall, pressure versus depth in the Chalk generally follows the hydrostatic gradient, although overpressures of 10–22 bars (Fig. 19) are observed at 1000 m depth (TNO & EBN SNS database), with a general northward increase. Overpressure is particularly high near the Ternaard diapir, where the Chalk is buried at 2800 m. These overpressures are linked to increased sedimentary loading during the Pliocene and Quaternary, as well as the low permeability of the formation caused by diagenetic cementation at depths greater than 1100 m; salt cementation may also contribute. The range of pressures indicates that vertical equilibration is limited and that the Chalk behaves as a low-permeability, semi-confined aquifer (Orozova-Bekkevold et al., 2021; Verweij et al., 2012). This suggests the presence of dynamic, basin-wide, semi-confined aquifer conditions: in areas where the Chalk can equilibrate, flow may occur across the basin, generally toward the north, driven by small hydraulic gradients. However, the observed overpressures indicate that during Pliocene and Quaternary sedimentary loading, the Chalk was unable to dewater rapidly, resulting in trapped water and elevated pressures.

The Lower Cretaceous Rijnland members (RN groups) consist of a mixture of clay and siltstones. They are normally pressured to only slightly overpressured (0–10 Mpa; Fig. 19; TNO & EBN SNS database), consistent with compaction of low-permeability rocks. The overlying Chalk Group, though of low permeability, is not an effective top seal and allows fluid pressures to equilibrate over geological times, while rapid sedimentary loading during the Pliocene and Quaternary contributed only minor additional overpressure (Verweij, 2003). In the Noord-Nederlands, Jurassic units (SK, SG, SL and AT Groups) are observed mainly in the Lower Saxony Basin and present similar overpressure trends, consistent with load-induced overpressuring of clay-rich rocks. Overpressures are likewise maintained by overlying low-permeability mudstones of the Upper Jurassic and Rijnland groups, suggesting limited lateral fluid movement. In the Jurassic-Lower Cretaceous formation, pressure dissipation occurs mainly through vertical expulsion of fluids from compacting layers toward the Chalk semi-confined aquifer, while lateral fluid flow is extremely restricted by the intrinsic low permeability of the formation.

The Triassic and Permian sequences consist of reservoir rocks (sandstones and carbonates) interbedded with sealing units (clays and evaporites), forming multiple pressure compartments. Overpressures reach up to ~80 bar in the Lower Saxony Basin and Lauwerszee Trough (Verweij et al., 2011), while structural highs such as the Groningen and Friesland platforms show only minor overpressure (~10 bar). These pressures are mainly controlled by the presence and sealing capacity of thick salt and shale layers (Pluymaekers, 2012), which strongly restrict basin-scale fluid circulation. Compartmentalization was further strengthened during Late Cretaceous–Early Paleogene inversion, when fault reactivation and uplift increased pore pressures and created additional structural barriers. Salt cementation in Triassic units also reduces permeability. As a result, fluids in Triassic and Permian formations are largely trapped, with flow occurring only episodically, as indicated by near-maximum pressures in several Triassic and Jurassic units. In the northern Netherlands, overpressure decreases toward western structural highs, where salt layers are thinner and more discontinuous. Despite compartmentalization, limited hydraulic communication persists, allowing slow lateral and upward flow from deeply buried overpressured zones toward structurally higher, lower-pressure areas in the west and south (Lee, 1999; Platt et al., 1993). The overall distribution suggests predominantly burial-induced upward flow through faults, with little influence from topography-driven flow under present-day conditions.

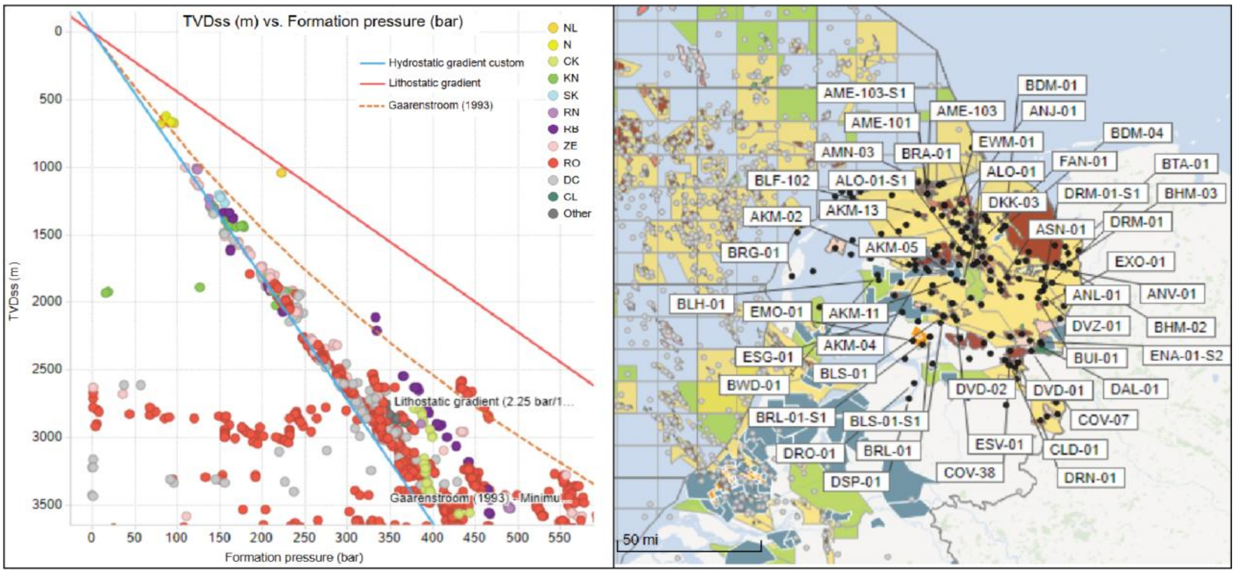

Figure 19: *Overpressure distribution in the northern Netherlands, from TNO & EBN SNS database. Left panel: Pressure vs. depth for selected formations, showing formation pressure in bars. The blue line indicates the hydrostatic gradient, while the brown line represents the minimum Leak-Off Pressure (LOP) trend. Right panel: Map of wells selected for pressure measurements across the Netherlands, with a focus on the northern onshore region. Well locations are used to derive the pressure-depth trends shown in the left panel and can be found in TNO & EBN SNS database.*

Salinity

Groundwater in Quaternary aquifers is generally fresh, with chloride concentrations typically below 30 mg/L (Broers et al., 2021; Stuyfzand, 1993). Composed mainly of permeable fluvial and aeolian sediments, these aquifers receive active meteoric recharge (Griffioen, 2024). Salinity increases toward the coast and offshore areas (Fig. 20), controlled by shoreline position, seawater intrusion and paleo–sea-level fluctuations (Delsman et al., 2015; Han et al., 2020).

Below 100 m depth, chloride concentrations range from 10 to ~10,000 mg/L (Delsman et al., 2023; TNO Grondwateratlas, 2017). Groundwater monitoring indicates that the transition from fresh to brackish water (~150 mg/L Cl^-) corresponds to the boundary between Quaternary continental aquifers and Neogene semi-confined marine deposits (Maassluis–Oosterhout–Breda formations, Fig. 20). This provides an estimate of the maximum depth of active meteoric recharge: fresh (~10–1,000 mg/L Cl^-), brackish (~1,000–15,000 mg/L Cl^-) and seawater (~19,000 mg/L Cl^-). Depth-contour maps of the fresh–brackish interface indicate that fresh groundwater occurs to a maximum depth of about 100–200 m in the north-eastern onshore Netherlands (Verweij, 2003). This is consistent with data from monitoring wells and the national NHI salinity model (Delsman et al., 2015). In the Breda Formation, salinity increases exponentially, ranging from 200 to 20,000 mg/L (Fig. 20). Primarily marine in origin, this water is partially freshened by overlying aquifers, with chemistry affected by mineral interactions and confined by Rupelian clay.

Deeper, confined aquifers, such as the Dongen and other pre-Rupelian units (Cretaceous, Jurassic, Triassic/Permian and Carboniferous), are generally saline (Griffioen et al., 2016), with chloride concentrations ranging from 1,000 to 150,000 mg/L. Overall, salinity increases markedly with depth. Palaeogene aquifers originally contained marine porewater, which was partially replaced by meteoric water during Tertiary emersion events (Glasbergen, 1981). However, present-day salinity reflects strong fluid–rock interactions and the presence of underlying saline formations. Elevated concentrations of bromide, lithium and boron in locations such as Asten and Nieuweschans indicate interactions with halite and residual brines, resulting in strong enrichment of water from salt diapirs (Glasbergen, 1981; Zuurdeeg & Coenegracht, 1986).

Deep-water samples from Upper Permian to Upper Cretaceous hydrostratigraphic units are hypersaline, chloride-dominated brines, with chloride concentrations up to 160,000 mg/L and minimum values above 40,000 mg/L. These waters are confined and ancient, reflecting processes such as halite dissolution, brine mixing and cation exchange, rather than recent recharge. Diagenetic evidence also indicates that meteoric water entered the Permian Rotliegend. As a result, fresh water is largely restricted to shallow Quaternary and Palaeogene aquifers in north-eastern Netherlands, while deeper units, including Dongen and Mesozoic–Carboniferous aquifers, remain naturally saline to hypersaline. Salt diapir subrosion, expulsion of saline fluids and fluid–rock interaction have contributed substantially to the salinization of these deeper reservoir units.

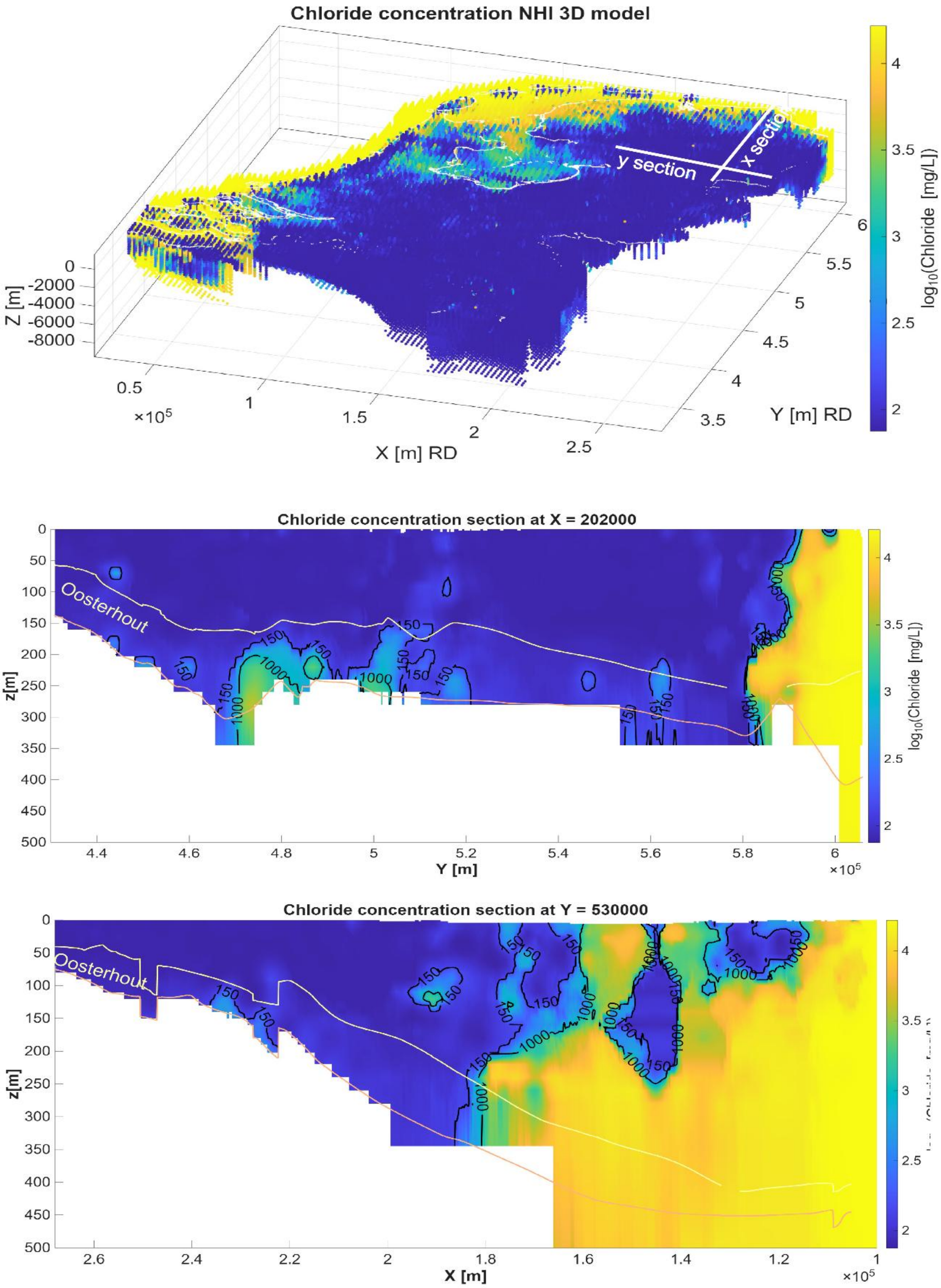

Figure 20. *Chloride concentration in the NHI 3D model (Delsman et al., 2023) with hydrostratigraphic layers. Top: 3D point cloud of chloride (log scale) distribution over the Netherlands. Middle: 2D Y-section at 540,000 m and bottom: 2D X-section at 210,000 m, showing contours at 150 mg/L (fresh–brackish) and 1000 mg/L (brackish–salt). These salinity transitions occur mainly within the Oosterhout Formation and the Breda Formation, which lies directly beneath the Oosterhout stratigraphic unit. Both units are clay-rich and act as aquitards in this area. The coordinate reference system is RD Netherlands, EPSG:28992.*

6.3.2 Parameterization of Geological and Hydrodynamic Properties

Hydraulic properties, overpressure and salinity were integrated into the TemisFlow™ model. The porosity (ϕ_0), permeability (k_0), overpressure and salinity values are derived from both the REGIS II and NHI hydrogeological frameworks, complemented by literature-based estimates for deeper formations (Table 5). The model was processed using backstripping following Li et al. (2024), allowing diapirs to evolve dynamically and rise to the surface over the 250 Myr timespan. These values represent present-day conditions; however, porosity and permeability evolve with depth according to the model's back stripping procedure.

Overpressures at the model boundaries define the hydraulic gradients that drive fluid flow within the system. At the southern boundary, variable overpressure is imposed, while the northern boundary is fixed at hydrostatic conditions. Over geological time, overpressure is modelled as a linear increase from 1.5 bar at the time of deposition to the present-day measured values at the boundaries (Table 5). Salinity is initially set to 50 mg/L NaCl for the entire geological history, with values updated over the last 2 Myr to those reported in Table 5. The parameters were iteratively tested and refined to reproduce observed pressure, porosity and permeability trends reported in the literature.

A 40 meter Zechstein sublayer was constructed within the model developed in the previous study, and an anhydrite lithology was implemented at the diapir location (map Fig. 21a). The porosity of the caprock at the diapir crest follows the anhydrite porosity–depth relationship, ranging from 1% to 4%. The permeability range between 0.5 and 0.001 md. The subrosion rate corresponds to the amount of salt dissolved within this Zechstein top layer, over time, expressed as thickness loss in m/Myr.

idx	code	Permeability k0 md	Porosity $\phi 0$	Anisotropy	Overpressure (bar)	[NaCl] (mg/L)
35	NUBX	5E3	0.4	0.5	1.5	50
34	NUDR + NUEE + NUKR	2.5	0.6	0.5	1.5	50
33	NUPE + NUURTY + NUDN	5E3	0.4	0.01	1.5	50
32	NUUR	2E4	0.4	0.5	1.5	50
31	NUAP	5E4	0.4	0.5	1.5	50
30	NUPZ-WAz1-2	5E4	0.4	0.5	1.5	50
29	NUPZc	5E3	0.5	0.01	1.5	50
28	NUPZ-WAz3	5E4	0.4	0.5	1.5	50
27	NUOT+NUMS	5E3	0.5	0.01	1.5	200
26	NUBRk1	0	0.5	0.5	1.5	5.000

25	NMRU + NMTO	2	0.6	0.1	5	5.000
24	NLDOBR	1E3	0.4	1	5	5.000
23	NLDOIE	2	0.6	0.1	5	5.000
22						50.000
21	CK	1E3	0.65	1	10	50.000
20						50.000
19						50.000
18						50.000
14	KN	2	0.6	0.1	10	100.000
13	S	5	0.6	0.1	10	100.000
12	ATPO	1.5	0.65	0.1	10	100.000
11	AT	1.5	0.65	0.1	10	100.000
10	RNK	5	0.6	0.5	30	100.000
9	RNMU	600	0.38	1	50	100.000
8	RNROU	100	0.5	1	50	100.000
7	RNRO1	1E-6	0.1	1	50	100.000
6	RNSOC.	5	0.6	0.1	50	100.000
5	RBM RBS	100	0.5	1	50	100.000
4	Top ZE (Anhydrite)	1	0.1	1	50	100.000
3	ZE	1E-6	0.1	1	50	100.000
2	RO	1E3	0.4	1	50	100.000
1	PreRO	5	0.6	0.1	50	100.000

Table 5. *List of lithological and hydraulic parameters used for each stratigraphic unit in the numerical model. The porosity (ϕ_0) and permeability (k_0) values correspond to their surface values, from which the depth-dependent variations are computed internally in TemisFlow. Overpressure and salinity ([NaCl]) are imposed as boundary conditions and the anisotropy term represents the vertical-to-horizontal permeability ratio.*

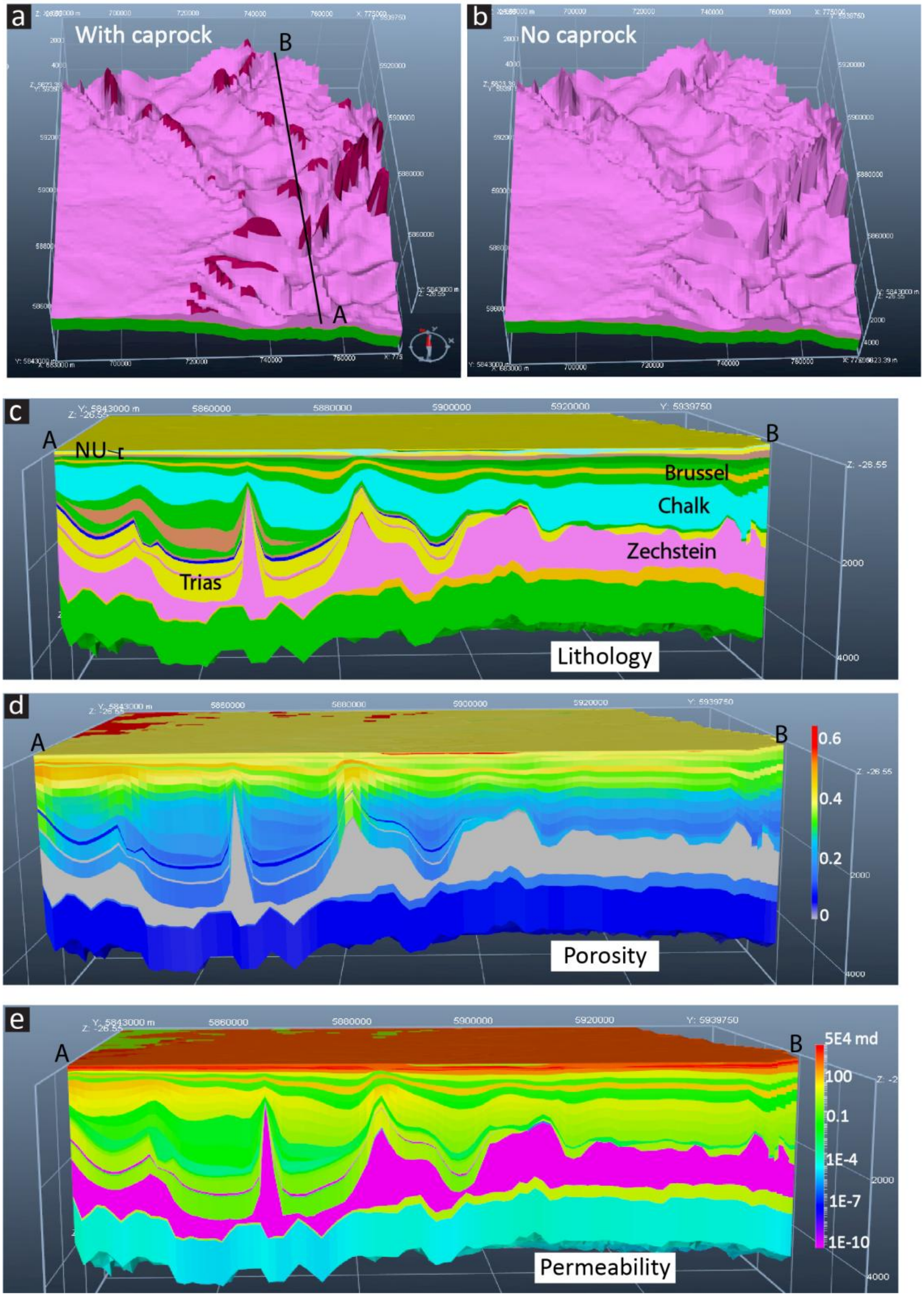

Figure 21. *Real-case basin-scale model scenarios. 3D TemisFlow^{TM} simulation for the northern Netherlands Zechstein diapirs. a) Top view of the model including a caprock over the major diapirs. b) Same model without caprock. c) Vertical section showing lithological distribution: sandy units in yellow, clay/marl in green, carbonates in turquoise; the main reservoirs above Zechstein salt are the Trias, Chalk, Brussels, and Upper North Sea Group (NU, location indicated in a). d) Same section displaying porosity distribution. e) Same section showing permeability distribution. At the southern boundary, variable overpressure is imposed, while the northern boundary is fixed at hydrostatic conditions.*

6.4 Result

After integrating all new geological, hydrodynamic and geochemical parameters into the TemisFlow™ model, the system was simulated over 250 Myr to reconstruct the temporal evolution of porosity and permeability up to present-day conditions (Fig. 21). These properties evolve dynamically through compaction and burial, following depth- and lithology-dependent relationships. The highest porosity and permeability values are observed in the main reservoir formations — the Trias, Chalk, Brussels sands and Upper North Sea Group (NU) — which consist primarily of sandy and carbonate lithologies (Fig. 21c–e). Due to their shallower position above the salt structures, these formations display local porosity and permeability maxima at the crest of the diapirs, where reduced burial depth and deformation enhance fluid circulation and potential subrosion activity.

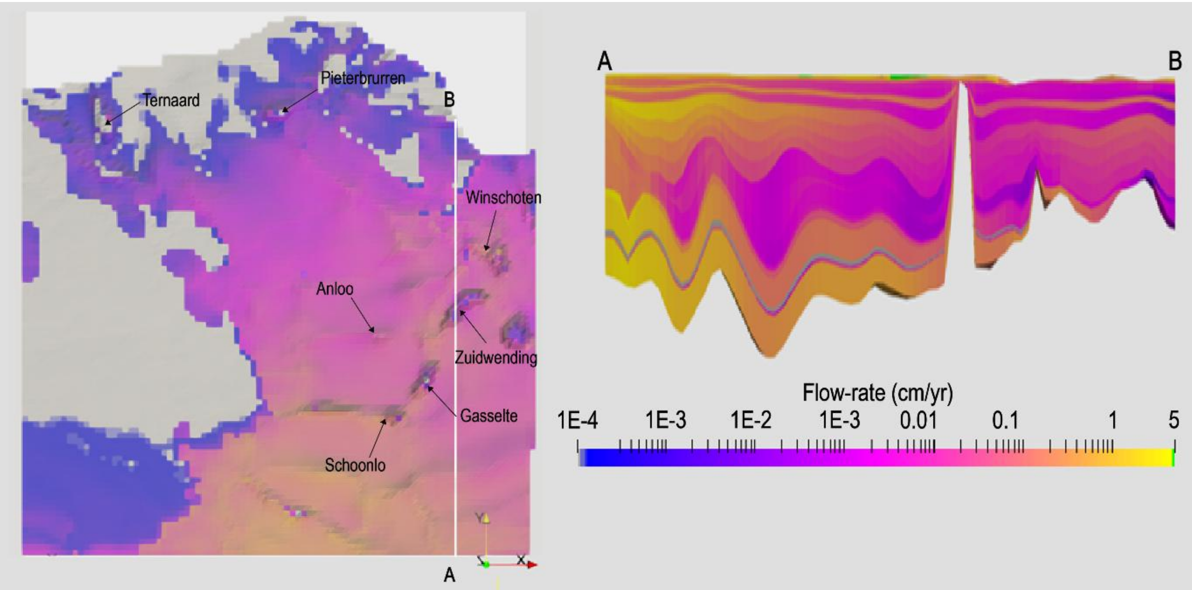

Figure 22. *Flow rate distribution in contact with, or directly above, the Zechstein layer. Left panel: Map view showing spatial variations in flow rate across the model domain. Flow is predominantly northward, with velocities on the order of m/ yr in the northern part of the domain and decreasing to mm/ yr in the south due to updated parametrization. Right panel: Cross-sectional view of the model illustrating flow rate variation with depth. Flow is concentrated in the main reservoir layers, particularly at the top of the Zechstein, highlighting preferential pathways for fluid migration. panel:*

6.4.1 Past subrosion rate

In the model, fluid flow in contact with the Zechstein layer is a primary control on subrosion rates (m/Myr). The average flow distribution over the simulated 250 Myr evolution (Fig. 22) shows a predominantly northward flow pattern following the regional hydraulic gradient. Flow velocities reach several meters per year in the north and gradually decrease southward to millimeters per year due to reduced permeability and connectivity. Flow is concentrated within the main reservoir formations, with higher subrosion rates where these permeable units directly overlie the Zechstein.

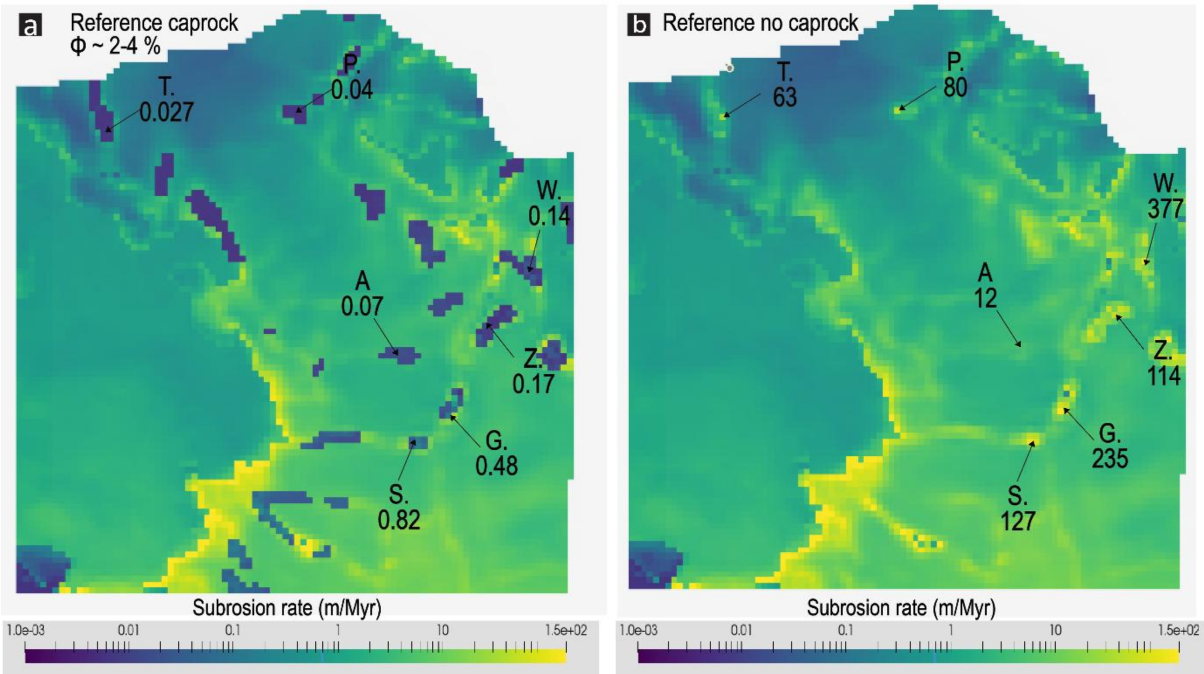

Figure 23. *Past subrosion rate distribution on top of the Zechstein salt structures— averaged over 250 Myr — in contact with, or directly above, the Zechstein layer. a) shows the distribution of subrosion rates for the model scenario including a caprock, while b) represents the scenario without a caprock. Abbreviations on the maps correspond to the locations used in Figure 22, with subrosion rate values indicated beneath each abbreviation.*

Subrosion intensity varies strongly depending on the presence or absence of a caprock (Fig. 23). In the no-caprock scenario (Fig. 23b), rates range from ~60 m/Myr in the north (Ternaard and Pieterburen diapirs) to ~235 m/Myr in the south (Zuidwendig, Gasselte, Schoonlo and Anloo diapirs), reflecting the influence of high flow velocities and shallow, well-connected reservoir units. The Winschoten diapir falls somewhat outside of these general ranges due to its very shallow interaction with a high-permeability aquifer present in one cell of the model grid, which locally enhances subrosion rates. When a caprock is included (Fig. 23a), subrosion rates decrease substantially to values on the order of 1 cm/Myr -1 m/Myr, with slightly higher rates in the south (~0.8 m/Myr) compared to the north (~0.03 m/Myr).

6.4.1 Present-day subrosion rate

The present-day configuration of the model predicts subrosion rates over a 2 Myr period, encompassing the last 1 Myr up to the present day and projecting 1 Myr into the future (Fig.24). The simulation uses hydrodynamic conditions constrained by measured data, representing the current groundwater flow, salinity distribution, and caprock properties.

In the no-caprock scenario, subrosion remains significant, with predicted rates ranging from ~10 to 140 m/Myr, depending on local flow intensity and reservoir connectivity (Fig. 24b). The highest values occur in the southern part of the domain, where reservoir formations are shallower and hydraulic gradients remain relatively high. In contrast, when a caprock is implemented, subrosion rates are drastically reduced, generally remaining below 1 m/Myr and reaching maximum values of ~1 m/Myr in localized zones above the southern diapirs (Fig. 24a).

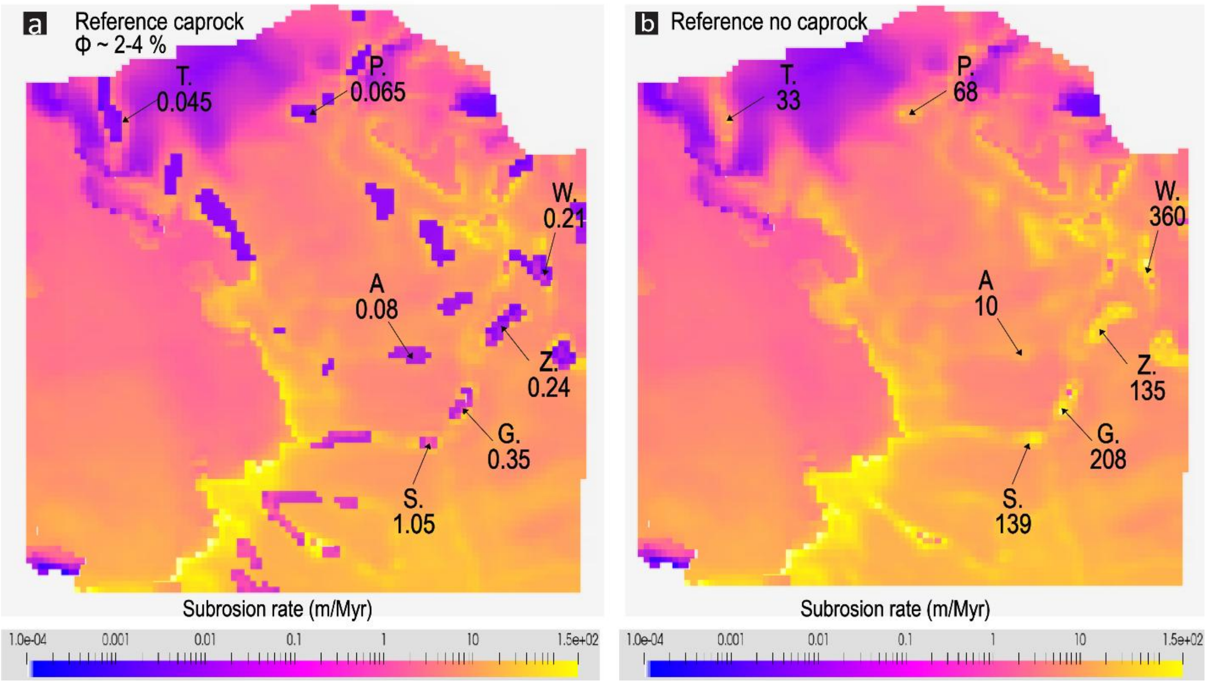

Figure 24. *Present-day subrosion rate distribution for model scenarios with and without a caprock. a) shows the scenario including a caprock, where subrosion rates are markedly reduced and limited to localized zones above the southern diapirs. b) illustrates the no-caprock scenario, showing higher subrosion rates associated with higher fluid circulation in shallow reservoir units. Abbreviations correspond to locations used in Figure 22.*

To test the model sensitivity to caprock porosity, two scenarios were evaluated with constant porosities of 1% and 5% (Fig. 25). For the model with a 1% caprock porosity, subrosion remains very limited, with rates ranging between 0.05 and 0.08 m/Myr, indicating an efficient barrier to fluid diffusion. In contrast, the model with a 5% caprock porosity shows locally enhanced dissolution above the diapirs, with subrosion rates reaching approximately 1 m/Myr in the southern diapirs (Fig. 25a).

Overall, the results indicate that, under current hydrodynamic conditions, large-scale dissolution is unlikely where an effective caprock is present. Active subrosion is instead restricted to areas where caprock integrity is limited or absent, highlighting the importance of caprock properties in controlling present-day and future salt stability.

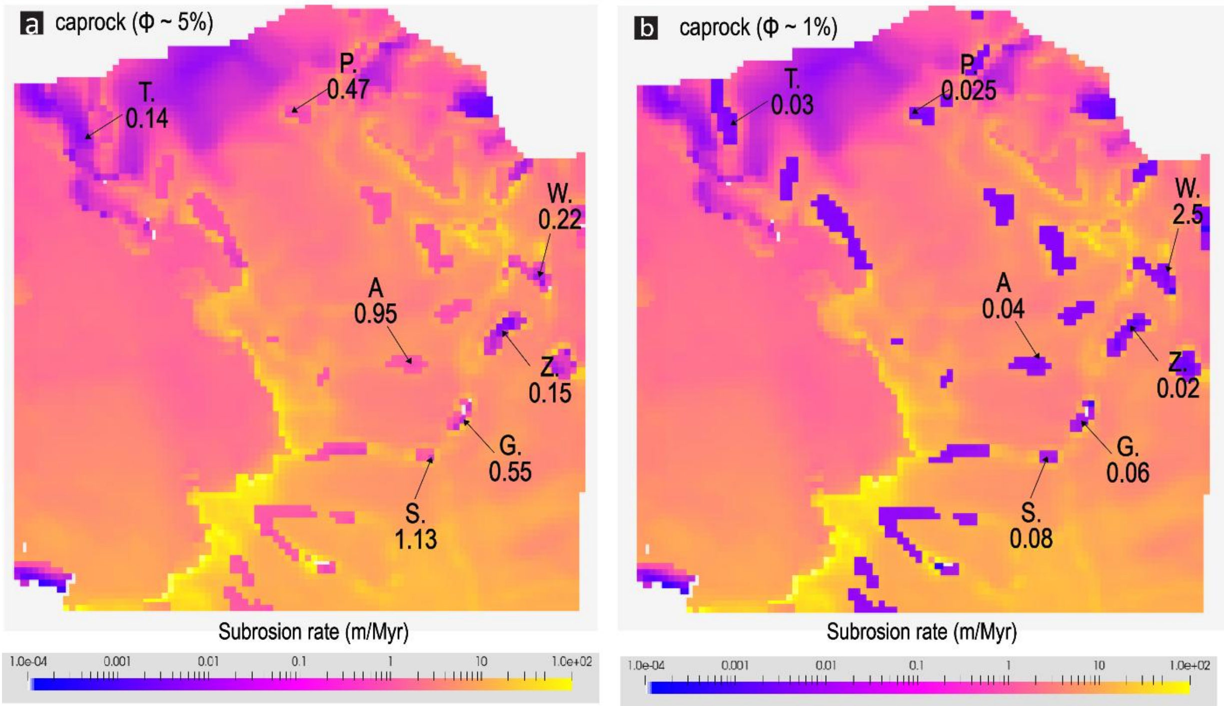

Figure 25. *Present-day subrosion rate distribution of the Zechstein layer for models with two different constant caprock porosity. a) shows the scenario with a caprock porosity of 5%, while b) represents the scenario with a caprock porosity of 1%. Abbreviations on the maps correspond to the locations used in Figure 22, with subrosion rate values indicated beneath each abbreviation.*

7. Comparison with real estimate from present condition.

Because hydrodynamic and hydrochemical conditions are difficult to constrain over 240 Myr of geological time, direct comparison of subrosion rate evolution with our simplified model is challenging. However, we can estimate a first-order average over the entire period, providing a relative order of magnitude for the subrosion process and enabling comparison with model data.

The overall subrosion rate can be estimated from the present-day caprock thickness and the proportion of non-soluble residues within the salt diapirs. This proportion, measured in several diapirs such as Zuidwendig, Schoonloo and Winschoten, is around 5%. The total thickness of salt removed through dissolution (*Ht*) can be approximated using:

$$H_t = \frac{H_{cp}}{p}$$

Where H_{cp} is the thickness of the caprock (non-soluble residues) and p is the fraction of non-soluble material in the diapir. Assuming a proportion of 5% and caprock thicknesses of 40 m, 30 m and 20 m for Zuidwendig, Schoonloo and Winschoten respectively, the total amount of salt dissolved is estimated at 800 m, 600 m, and 400 m over the last 240 Myr. This corresponds to average long-term subrosion rates of approximately 3.3 m/Myr, 2.5 m/Myr and 1.7 m/Myr, respectively. Note that this does implicitly assume that the caprock was formed directly after deposition.

The model results can also be compared with Almalki et al. (2023), who quantified salt movement and subrosion using a mass-balance approach based on seismic and well data from sediments surrounding diapirs. “Withdrawal basins” with increased sediment thickness due to salt migration were identified and the difference from normal thickness was used to estimate the total salt column, including subroded portions of Northern Netherlands Diapirs (Zuidwendig, Winschoten, Slochteren). Their study reports subrosion rates in the northern Netherlands of 2–10 m/Myr, with an average of ~4 m/Myr, consistent with estimates derived from present-day caprock thickness and residual salt. This confirms that sediment-based mass-balance methods may provide qualitative, but robust long-term constraints on salt dissolution, complementing caprock observations and hydrodynamic modelling.

These results align with the diffusion-controlled regime observed in the model for capped diapirs, indicating that subrosion in the northern Netherlands has remained moderate over geological time (from centimetre- to metre-scale per Myr). In our model, subrosion rates are slightly lower, ranging from 0.5 cm to 1 m/Myr depending on porosity, salt thickness, and salinity in the presence of a caprock. The process appears largely governed by caprock properties and by the region’s low groundwater flow at depth.

It should be noted that our model represents the extreme ends of this spectrum of subrosion rates, effectively illustrating potential best- and worst-case scenarios for subrosion. Moreover, the relatively low regional resolution of the model can lead to either overestimation or underestimation of subrosion rates. This is primarily because the coarse resolution does not always allow for realistic connections between diapirs and adjacent aquifers, as would occur in nature. Additionally, simplifications made during the interpretation phase of the national model, combined with uncertainties in layering boundaries, further contribute to these potential discrepancies. Addressing these limitations will be crucial in future modelling phases to improve accuracy and reliability. Although the model’s resolution is constrained by its regional scale, and it does not account for the formation or temporal evolution of caprock thickness, it still provides a robust first-order, order-of-magnitude estimate and valuable insight.

Looking forward, our modelling results suggest that future dissolution rates are unlikely to be strongly influenced by variations in fluid flow and will instead depend primarily on caprock thickness and intrinsic properties. Consequently, realistic long-term subrosion estimates for the northern Netherlands should focus on scenarios involving a well-developed caprock with variable thicknesses and porosity matching individual conditions for each of all the diapirs in the targeted depth range.

Conclusions and Recommendations

This project has advanced the understanding of the geological and hydro-chemical evolution of Zechstein salt diapirs in the Netherlands by building directly on the objectives of the two work packages. The first work package generated a new dataset of information for the Zechstein distribution of lithologies, providing detailed subunit descriptions, thicknesses and structured metadata. Two new maps were produced, showing total salt thickness and total non-salt thickness, providing essential spatial constraints that refine previous models and highlight significant regional heterogeneity. Results show that salt thickness increases northward, while the south-eastern regions are dominated by non-salt lithologies. The analysis also identified the presence of distinct caprock units of different lithologies, capping many diapirs and revealed that caprock thickness is depth-dependent, ranging from approximately 5–20 meters at depth to 30–80 meters near the surface, reflecting the cumulative impact of subrosion over the last ~240 million years.

In the second work package, the project advanced the previous research by implementing better hydro-chemical conditions for subrosion and integrating updated lithological data, hydrodynamic boundary conditions and salinity distributions. Conceptual models were first developed to assess the sensitivity of subrosion rates to individual parameters, including caprock thickness, porosity, aquifer salinity and groundwater flow. These models were complemented by the first analytical solution for estimating subrosion rate evolution over geological timescales. Building on these insights, a regional, basin-scale model covering the northern Netherlands diapirs region was developed and constrained using nature-based, but simplified datasets for the entire scale of northern Netherlands. The results demonstrate that incorporating realistic caprock properties yields subrosion rates that closely match observed values, although they remain slightly underestimated (1 cm/Myr to 1 m/Myr). In contrast, models that neglect caprock overestimate subrosion by up to ~150 m/Myr. This highlights the critical role of caprock properties in controlling fluid transport and long-term diapir stability.

The results underscore the necessity of high-resolution, case-by-case geological studies to accurately model subrosion in salt diapirs. Moreover, future work should focus on improving the characterization of caprock properties at a petrological level, including mineralogical and porosity variations, to allow better calibration and further constrain subrosion rates for individual diapirs. Combining detailed geological data with advanced hydro-chemical and thermo-mechanical models will enhance predictive capabilities, enabling more accurate assessments of diapir evolution and stability. In addition, developing more sophisticated formulations to account for reactive fluid transport and caprock formation over time would provide stronger constraints and reduce the error bars of the predicted subrosion values. These insights provide a solid foundation for future studies of complex salt systems, demonstrating that while regional models are valuable, local geological variability is crucial to capture the processes that govern long-term diapir behavior and stability.

References

Al-Halbouni, D., Holohan, E. P., Taheri, A., & Dahm, T. (2017, April). Distinct Element modeling of geophysical signatures during sinkhole collapse. In EGU General Assembly Conference Abstracts (p. 922).

Almalki, B. A. S., Bartol, J., & Matenco, L. (2023). Zechstein salt structures evolution in the north-eastern Netherlands. Department of Earth Sciences, 36.

Atlas, S. P. B. (2010). Petroleum Geological Atlas of the Southern Permian Basin Area.

Bartol, J., & Vuorio, K. (2025). Safety assessment for a geological disposal facility in domal salt: The Dutch case. Geomechanics for Energy and the Environment. (in press)

Broers, H. P., Cvetkovic, V., & Griffioen, J. (2021). Paleoclimate signals and groundwater age distributions: Evidence from Quaternary aquifers. Water Resources Research, 57(9), e2020WR029058. https://doi.org/10.1029/2020WR029058

Delsman, J. R., Mulder, T., Verastegui, B. R., Bootsma, H., Zitman, P., Huizer, S., & Oude Essink, G. H. P. (2023). Reproducible construction of a high-resolution national variable-density groundwater salinity model for the Netherlands. Environmental Modelling & Software, 164, 105683.

Delsman, J. R., Oude Essink, G. H. P., van Baaren, E. S., & Griffioen, J. (2015). Saline groundwater–surface water interaction in coastal lowlands: Processes and modelling considerations. In Proceedings / Netherlands Hydrological Society. https://www.hydrology.nl/images/docs/dutch/2015.06.15_Delsman.pdf.

Daudré, B., & Cloetingh, S. A. P. L. (1994). Numerical modelling of salt diapirism: Influence of the tectonic regime. Tectonophysics, 240, 59-79. https://doi.org/10.1016/0040-1951(94)90264-X

Geluk, M. C., Wong, T. E., Batjes, D. A. J., & De Jager, J. (2007). Permian. Geology of the Netherlands, 63-83.

Glasbergen, P. (1981). Extreme salt concentrations in deep aquifers in the Netherlands. Science of the Total Environment, 21, 251–260. https://doi.org/10.1016/0048-9697(81)90038-0

Griffioen, J. (2024). History of the hydrogeochemical study of groundwater in the Netherlands and the research motives. Hydrogeology Journal, 32, 679–689. https://doi.org/10.1007/s10040-023-02736-0

Han, D., et al. (2020). Groundwater salinization and flushing during glacial–interglacial cycles: Implications for Quaternary aquifers. Water Resources Research, 56(11), e2020WR027879. https://doi.org/10.1029/2020WR027879

Chen, J., Hunfeld, L. B., Niemeijer, A. R., & Spiers, C. J. (2023). Fault weakening during short seismic slip pulse experiments: The role of pressurized water and implications for induced earthquakes in the Groningen gas field. Journal of Geophysical Research: Solid Earth, 128(2), e2022JB025729.

Hummelman, J., Maljers, D., Menkovic, A., Reindersma, R., Vernes, R., & Stafleu, J. (2019). Totstandkomingsrapport hydrogeologisch model (regis ii). TNO-Geologische Dienst van Nederland, Utrecht, TNO-rapport, R11654.

Lauwerier, W., 2022. The evolution of the Zechstein salt diapirs in the north-eastern Netherlands., Internship research for Earth, Life and Climate. Utrecht University, Utrecht.

Lee, M., Aronson, J. L., & Savin, S. M. (1989). Timing and Conditions of Permian Rotliegende Sandstone Diagenesis, Southern North Sea: K/Ar and Oxygen Isotopic Data1. AAPG bulletin, 73(2), 195-215.

Li, M., Collard, N., Schueller, S., Matenco, L., Nader, F. H., Beekman, F., Cacas, M.-C., & Bartol, J. (2024). Quantitative modelling of diapirism and geochemical evolution of the subrosion process of salt domes in the northeast Netherlands for radioactive waste disposal. Utrecht University & IFP Energies Nouvelles. Ministry of Infrastructure and Water Management.

Orozova-Bekkevold, I., & Petersen, T. G. (2021). Numerical forward modelling of the overpressure build-up in the Cenozoic section of the Central Graben in the North Sea. Journal of Petroleum Exploration and Production, 11(4), 1621–1642.

Platt, J. D. (1993). Controls on clay mineral distribution and chemistry in the early Permian Rotliegend of Germany. Clay Minerals, 28(3), 393–416.

Pluymaekers, M. P. D., Kramers, L., Van Wees, J. D., Kronimus, A., Nelskamp, S., Boxem, T., & Bonté, D. (2012). Reservoir characterisation of aquifers for direct heat production: Methodology and screening of the potential reservoirs for the Netherlands. Netherlands Journal of Geosciences, 91(4), 621–636.

Remmelts, G., Muyzert, E., van Rees, D. J., Geluk, M. C., de Ruyter, C. C., & Wildenborg, A. F. B. (1993). Evaluation of salt bodies and their overburden in the Netherlands for the disposal of radioactive waste, b. Salt movement: Report to Rijks Geologische Dienst.

Stuyfzand, P. J. (1993). Hydrochemistry and hydrology of the coastal dune area of the Western Netherlands (PhD thesis). Vrije Universiteit Amsterdam. https://research.vu.nl/files/75835105/214.pdf

TNO & EBN. (2020). Pressure SNS database: Southern North Sea – formation pressure, leak-off pressure and temperature data for ~1,145 wells [Database and web interface]. Available via NLOG / EBN Spotfire interface. https://www.ebn.nl

TNO – Geological Survey of the Netherlands. (2015). Integrated pressure information system for the onshore and offshore Netherlands: Final report (Report No. R10065, 83 pp.). (Project TKIG01002).

Verweij, J. M. (1999). Application of fluid flow systems analysis to reconstruct the post-Carboniferous hydrogeohistory of the onshore and offshore Netherlands. Marine and Petroleum Geology, 16(6), 561-579.

Verweij, H., Simmelink, E., & Underschultz, J. (2011). Pressure and fluid flow systems in the Permian Rotliegend in the Netherlands onshore and offshore. In The Permian Rotliegend of the Netherlands (SEPM Special Publication No. 98, pp. 247–263). SEPM. https://doi.org/10.2110/pec.11.98.0247

Verweij, J. M., Simmelink, H. J., Underschultz, J., & Witmans, N. (2012). Pressure and fluid dynamic characterisation of the Dutch subsurface. Netherlands Journal of Geosciences, 91(4), 465–490.

Verweij, J. M. (2003). Fluid flow systems analysis on geological timescales in onshore and offshore Netherlands: With special reference to the Broad Fourteens Basin [PhD thesis – Research external, graduation internal, Vrije Universiteit Amsterdam]. NSG.

Verweij, H., Oude Essink, G., Hartog, N., & Zaadnoordijk, W. J. (2025). Hydrogeology, Chap. 13, in Geology of the Netherlands. Amsterdam University Press.

Vis, G. J., & Verweij, J. M. (2014). Geological and geohydrological characterization of the Boom Clay and its overburden. COVRA NV Report OPERA-PU-TNO411 (Utrecht). Ziegler, K. (2006). Clay minerals of the Permian Rotliegend Group in the North Sea and adjacent areas. Clay minerals, 41(1), 355-393.

Zuurdeeg, B. W., & Coenegracht, Y. M. A. (1986). Genesis of the mineral water of Nieuweschans. University of Utrecht, Department of Geochemistry, report.

Geological Survey of the Netherlands (TNO). (n.d.). Groundwater Quality Viewer (Grondwateratlas). https://www.grondwatertools.nl/gwatlas

Appendices

Appendix 1 – Corrected Inventory of Zechstein Intra-Salt Lithologies and Seismic Data

Appendix 1 presents the corrected inventory dataset of Zechstein intra-salt lithologies and seismic data used in the study. All data are provided within the archive “inventory.zip”, which contains two main folders: “wells” and “seismic” (Fig. A.1).

- **Wells folder:** The wells folder is organized into two subdirectories: “offshore” and “onshore” wells. Within each, you will find: Log data in XLS format, containing the top and bottom depths of each interval, interval thickness, the NLOG code with its full name, the identified Zechstein lithology, and its classification category (Salt / Non-Salt / Caprock), consistent with the descriptions in Section 1.2. Each log file is accompanied by a PNG image of the corresponding log for visual reference.

A “histogram “ folder containing images of histograms illustrating the proportions of Salt, Non-Salt, and Caprock lithologies. These histograms correspond to those shown in Figures 2 through 9 of the report.

- **Seismic folder:** The seismic folder contains a single PDF file named “seismic_inventory_diapirs.pdf”. This PDF includes maps of seismic lines crossing the main diapirs with tops shallower than 1000 m depth, as well as seismic profiles with key interpreted horizons, illustrating the structure and geometry of the major diapirs.

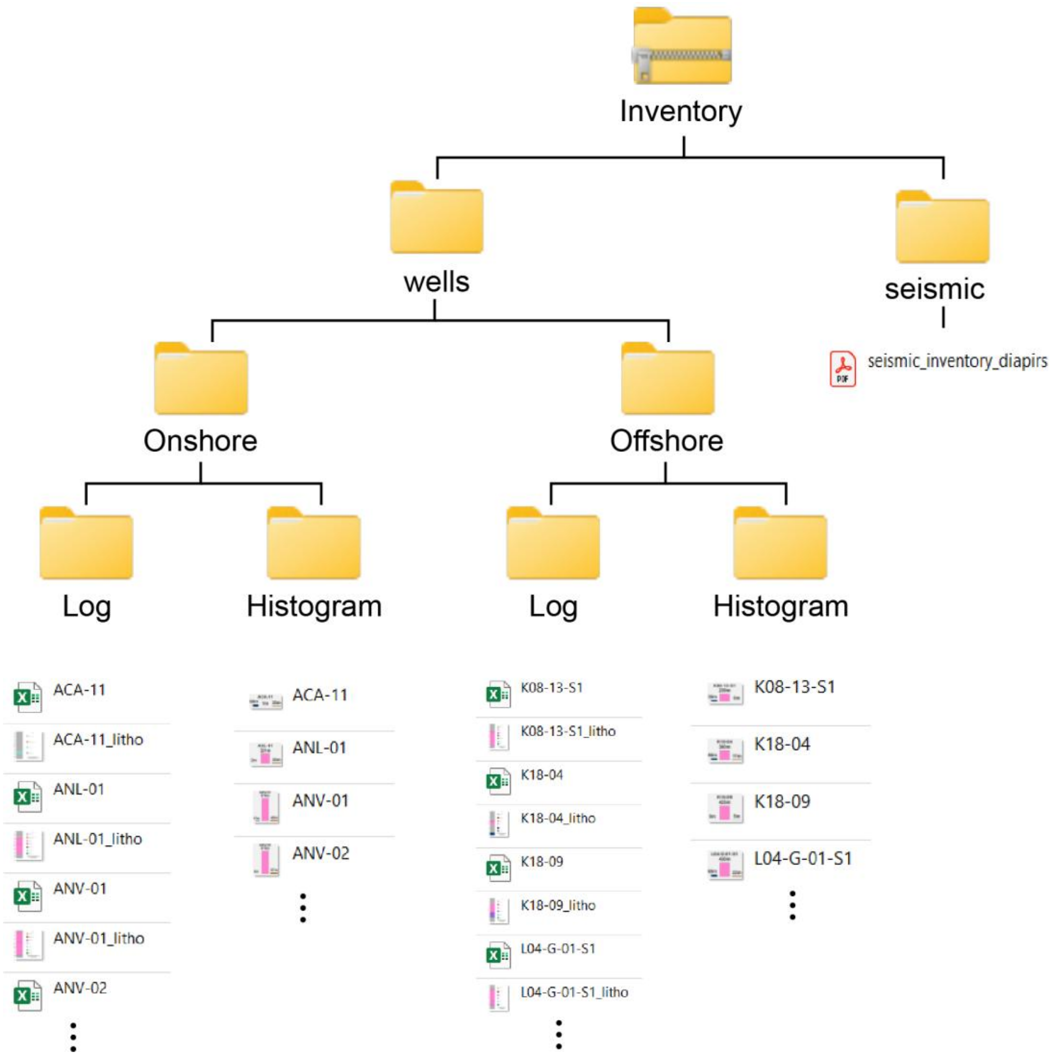

Figure A.1: *Folder path diagram illustrating the organization of the inventory dataset.*

Appendix 2 – Dataset for Salt Dome Mapping and Salt Thickness Distribution

Appendix 2 presents the dataset used for Section 2, which focuses on the mapping of salt domes and the distribution of salt thickness (see page 22). The dataset and corresponding maps are provided in a zip file named “maps” (Fig. A.2). This archive is organized into two main folders: “data” and “map.”

Within each folder, you will find:

- **Data folder:** Contains the well data used to compute the maps, provided in both CSV and Shapefile formats. These datasets include the spatial locations and key attributes of the wells contributing to the mapping of salt and non-salt units.

- Maps folder: Contains subfolders named “Salt” and “Non-Salt,” which include the grid maps representing the thickness distribution of salt and non-salt lithologies (pages 23–24). Each map is provided in both GeoTIFF format (indicated with the suffix _gis), for use in GIS software, and ZMAP format, for use in Petrel or Mapviewer. In addition, a PDF version of each map is included for easy viewing and reference.

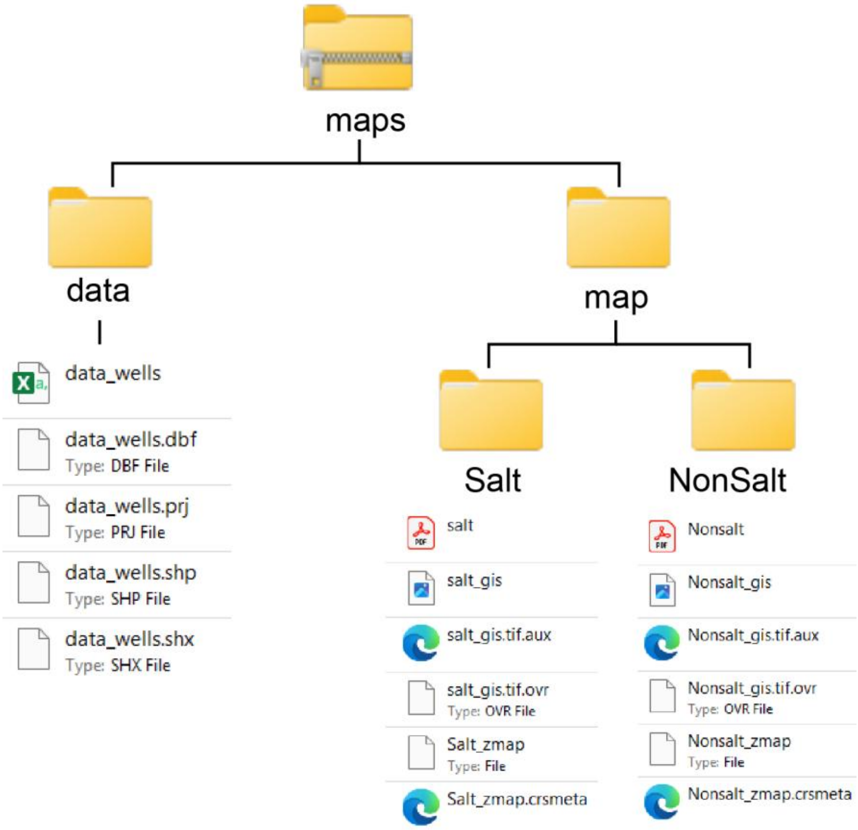

Figure A.2: *Folder path diagram illustrating the organization of the maps dataset used for building the "Salt" and "Non-Salt" thickness maps.*

Appendix 3 – Project Files and Output Grids for OpenFlow 3D Subrosion Simulations

Appendix 3 presents the project files and output grids used in Section 6, which discusses the 3D simulations of salinity evolution and groundwater circulation at the basin scale for the NE Netherlands onshore area. All simulation files and results are provided in a zip file named "Openflow" (Fig. A.3). The archive is organized into two main folders: "Project" and "Grids". Within each folder, you will find:

Project folder: Contains the complete numerical model used for the simulations, provided in OFL TemisFlow™ project format. This includes the model configuration, input parameters, and setup files used to generate the subrosion rate outputs and salinity flow fields discussed in Section 6.

Grids folder: Provides the evaluated diapir subrosion rates (m/Myr) in both GIS and XYZ grid formats. The folder is divided into two subdirectories corresponding to the reference models described in Section 6.4.1: Caprock_model and Salt_model.

Each of these two model folders contains a subfolder for the average flow distribution over the 250 Myr simulated evolution (past). A subfolder for the present-day subrosion rate distribution (present). Time-slice folders include:

- Subrosion rate grids in XYZ format.

- Subrosion rate grids in GeoTIFF format for use in GIS software.

These datasets correspond to the subrosion analyses and outputs presented in Section 6.4.

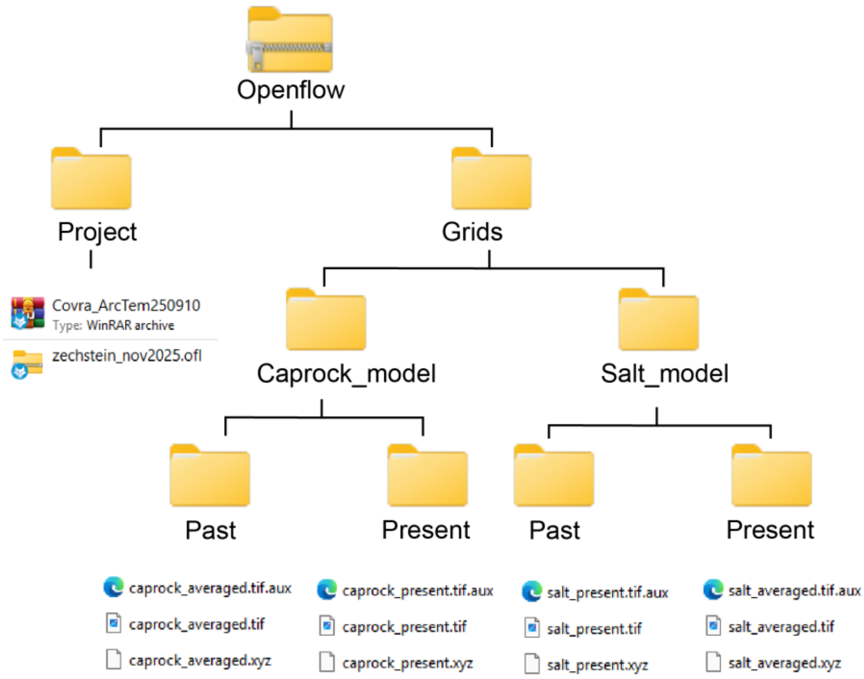

Figure A.3*: Folder path diagram illustrating the organization of the OpenFlow project files and output grids.*